

# Trends in Nanophotonics-Enabled Optofluidic Biosensors

Juan Wang, Stefan A. Maier,\* and Andreas Tittl\*

Optofluidic sensors integrate photonics with micro/nanofluidics to realize compact devices for the label-free detection of molecules and the real-time monitoring of dynamic surface binding events with high specificity, ultrahigh sensitivity, low detection limit, and multiplexing capability. Nanophotonic structures composed of metallic and/or dielectric building blocks excel at focusing light into ultrasmall volumes, creating enhanced electromagnetic near-fields ideal for amplifying the molecular signal readout. Furthermore, fluidic control on small length scales enables precise tailoring of the spatial overlap between the electromagnetic hotspots and the analytes, boosting light-matter interaction, and can be utilized to integrate advanced functionalities for the pre-treatment of samples in real-world-use cases, such as purification, separation, or dilution. In this review, the authors highlight current trends in nanophotonics-enabled optofluidic biosensors for applications in the life sciences while providing a detailed perspective on how these approaches can synergistically amplify the optical signal readout and achieve real-time dynamic monitoring, which is crucial in biomedical assays and clinical diagnostics.

the need for compact, portable, and field-deployable sensor devices has created significant interest around miniaturized and automated approaches for on-chip early diagnosis of diseases and general health monitoring.<sup>[8,9]</sup> Benefiting from advances in nanotechnology and micro/nanofluidic techniques, optofluidic sensors have seen intense development, with the goal of ultimately integrating nanophotonics and fluidics in one compact and portable chip. This unique combination not only amplifies the signal readout through engineering of the resonant coupling of nanophotonic structures with matter and the spatial overlap of nanoscale hotspots of the electromagnetic near-fields with analytes of interests, but can additionally perform analyte pre-treatment on-chip and mimic in-vivo environments for investigating organ-on-a-chip models.<sup>[6,10,11]</sup>

Nanophotonic chips composed of nanostructured plasmonic and/or dielectric materials can dramatically boost analyte sensitivity due to their strong light confinement and near-field enhancement at the nanoscale, which enables efficient overlap with small target biomolecules. In this review, we will first present the physical fundamentals and mechanisms of nanophotonics-enabled sensing, emphasizing the surface plasmon resonances (SPRs) and localized surface plasmon resonances (LSPRs) found in metals, as well as Mie-type resonances in all-dielectric nanostructures and recently introduced metasurfaces based on photonic bound states in the continuum (BICs). These nanophotonic approaches are compared to highlight their characteristic features and advantages for the design of optical sensors from the point of view of resonance frequency tuning, quality ( $Q$ ) factor engineering, and near-field enhancement. Furthermore, we will introduce the leading transduction schemes of optical sensors, including refractometry, surface-enhanced fluorescence (SEF) spectroscopy, surface-enhanced Raman spectroscopy (SERS), and surface-enhanced infrared absorption spectroscopy (SEIRAS).


Through the integration of micro/nanofluidic channels onto the nanophotonic chips, target analytes can be precisely trapped and confined into the electromagnetic hotspots to maximize light-matter interaction and boost sensitivity. By incorporating advanced fluidic manipulation, such as flow-through geometries<sup>[12,13]</sup> and electric field driven flow,<sup>[14,15]</sup> the transport of analytes of interests can be tailored to overcome the diffusion limit and accelerate the binding time, thus realizing ultratrace analysis with low detection limits down to single molecule level. Moreover, careful design of the fluidic compartment is essential for realizing multifunctionality for the pre-treatment

## 1. Introduction

There is strong demand for developing efficient and reliable sensing platforms to meet global challenges in personalized healthcare, including real-time biomedical assays and point-of-care (POC) clinical diagnostics.<sup>[1–3]</sup> To enable a new generation of healthcare devices, capabilities such as high specificity, ultrahigh sensitivity, multiplexing, non-invasive label-free operation, and real-time monitoring are highly desirable.<sup>[4–7]</sup> In addition,

J. Wang, S. A. Maier, A. Tittl  
Chair in Hybrid Nanosystems  
Nanoinstitute Munich  
Faculty of Physics  
Ludwig-Maximilians-Universität München  
80539 München, Germany  
E-mail: stefan.maier@physik.uni-muenchen.de;  
andreas.tittl@physik.uni-muenchen.de

S. A. Maier  
The Blackett Laboratory  
Department of Physics  
Imperial College London  
London SW7 2AZ, UK

 The ORCID identification number(s) for the author(s) of this article can be found under <https://doi.org/10.1002/adom.202102366>.

© 2022 The Authors. Advanced Optical Materials published by Wiley-VCH GmbH. This is an open access article under the terms of the Creative Commons Attribution License, which permits use, distribution and reproduction in any medium, provided the original work is properly cited.

DOI: 10.1002/adom.202102366

of analytes, including filtration, separation, enrichment, and amplification, as well as for on-chip culturing and associated in-vitro studies. To emphasize the synergy between nanophotonic and fluidic engineering, we will focus on different facets of fluidic compartment integration, such as optofluidic chip bonding, microfluidic channel design for multiplexing, high throughput and automated analysis, nanofluidic channel creation, acceleration of mass transport, as well as the critical element of realizing fluidic compartments with multifunctionality. Finally, the challenges and opportunities of optofluidic sensors will be summarized to provide a perspective on the development of a new-generation of on-chip, portable optofluidic sensors for fundamental studies in the life sciences as well as for commercialized diagnostic devices at the point-of-care.

## 2. Nanophotonics

Photonic nanostructures composed of metals and/or high refractive index dielectrics can concentrate light into small volumes and produce greatly amplified electromagnetic near-fields (so-called hotspots), significantly boosting light-matter interactions. Therefore, resonant nanophotonic systems can act as ideal building blocks for label-free, non-invasive, and multiplexed optical sensing platforms, setting them apart from other techniques such as electrochemical sensing and enzyme-linked immunosorbent assays (ELISA).<sup>[16–18]</sup> Plasmonic sensor approaches have played a dominant role in the past decades, but face limitations for some sensing applications due their intrinsic absorption losses, especially in heat-sensitive systems where light-induced heat generation and transfer can play a crucial role.<sup>[19]</sup> To overcome this limitation, nanostructured high refractive index dielectrics have been introduced as optical sensors with low losses, while showing comparable sensitivity with plasmonics for many relevant applications.<sup>[20,21]</sup> In the following, we will briefly present the physical fundamentals of how nanostructured plasmonic and dielectric materials can simultaneously deliver enhanced near-fields and far-field spectra with controllable resonance frequency and  $Q$  factor.

### 2.1. Plasmonics

Plasmonic systems leverage the resonantly driven coherent oscillations of conduction electrons in metals and are commonly implemented either as propagating electromagnetic surface waves at metal/dielectric interfaces (surface plasmon resonances, SPRs) or as excitations in subwavelength metallic particles (localized surface plasmon resonances, LSPRs).<sup>[22]</sup> In general, SPRs are supported on interfaces with opposite signs of the real part of the permittivity, producing a characteristic wave pattern and surface charge distribution (Figure 1a). Based on Maxwell's equations and the boundary conditions at a planar metal/dielectric interface, the dispersion relation of a SPR can be calculated to:<sup>[23]</sup>

$$k_{\text{SPR}} = k_0 \sqrt{\frac{\epsilon_d \epsilon_m}{\epsilon_d + \epsilon_m}} \quad (1)$$

where  $\epsilon_d$  and  $\epsilon_m$  are the permittivity of the dielectric material and the metal,  $k_0$  is the free-space wavevector, and  $k_{\text{SPR}}$  denotes the SPR wavevector. Importantly, there is a significant momentum mismatch between the SPR dispersion and the light line, preventing direct excitation of the SPR from the far-field (Figure 1b, top). One way to overcome this constraint is by prism coupling in the well-known Kretschmann configuration (Figure 1b, bottom).<sup>[24,25]</sup> Additionally, the scattering from a geometrical defect on the surface<sup>[26]</sup> and a periodic corrugation in the metal surface<sup>[27,28]</sup> can be used to generate SPRs. Despite the propagating nature of the SPR, the electromagnetic near-fields associated with the wave still decay exponentially away from the surface, leading to field confinement close to the metal/dielectric interface.

For nanophotonic applications with more demanding near-field control requirements, LSPRs can concentrate electromagnetic energy in all three spatial dimensions by confining the coherent electron oscillations to subwavelength metal nanoparticles (Figure 1c). From an analytical standpoint, the photonic characteristics (e.g., near-field distribution, absorption and scattering cross-sections) of LSPRs supported on spherical metallic nanoparticles can be studied by Mie theory, where the internal and scattered electromagnetic fields are expressed as linear combinations of spherical harmonics.<sup>[29]</sup> Going beyond simple particle shapes, introducing nano-gaps into plasmonic structures can produce substantially higher near-fields (Figure 1d). For instance, nanogaps can be formed in carefully spaced nanoparticle pairs, between a nanoparticle and an extended metal film, where the distance is often controlled through a self-assembled molecular layer, or realized as individual or periodic nanoslits.<sup>[30]</sup> Plasmonic geometries have been applied to design a variety of optical sensors working under different sensing principles.<sup>[31–33]</sup> Individual plasmonic nanoobjects can be arranged periodically to harness radiative coupling and collective oscillation effects, enabling additional degrees of freedom for tailoring the near-fields as well as the resonance position and linewidth.<sup>[34–39]</sup> The field confinement of both SPR and LSPR approaches can be described by a characteristic decay length  $\delta_d$ . For SPRs,  $\delta_d$  is roughly on the order of half of the resonance wavelength (i.e., a few hundred nanometers), which is significantly larger than for LSPRs (e.g., about 20 nm for a spherical gold particle with a diameter of 30 nm at the electric dipole resonance).<sup>[40]</sup> Thus, for bulk refractive index sensing (where the entire volume adjacent to the resonant structure is filled with analyte), the SPR scheme gives rise to at least an order of magnitude higher sensitivity than that of LSPR-based sensors.<sup>[41]</sup> Even though a variety of plasmonic biosensors based on the Kretschmann configuration have already been commercialized, they are often still bulky and therefore not ideally suited for POC diagnostics.<sup>[42]</sup> In addition, when detecting ultrathin layers of adsorbed molecules, LSPR-based systems with smaller  $\delta_d$  are often advantageous, since they concentrate most of their detection volume close to the surface.<sup>[43,44]</sup> When trying to resolve minute spectral resonance shifts in response to extremely low analyte concentrations, engineering resonances with narrow linewidth is another crucial factor for optimizing sensor performance. One prominent approach for overcoming these limitations in plasmonics is the use of Fano resonances<sup>[45,46]</sup> supported on specifically designed ensembles

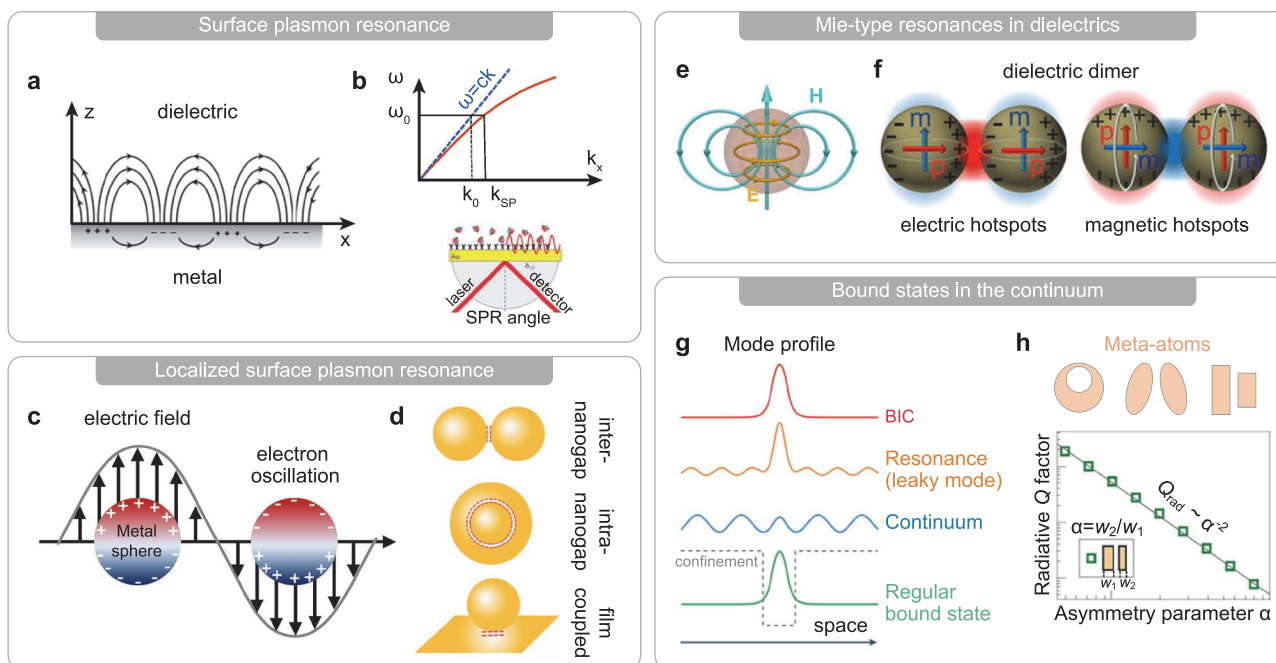


**Figure 1.** Fundamental aspects of nanophotonics. a) Illustration of SPR propagation at a metal/dielectric interface with the characteristic electromagnetic surface wave and charge distribution. b) The SPR dispersion curve shows a momentum mismatch between the light line and the plasmon, preventing direct excitation. Sketch of the Kretschmann configuration for exciting SPRs from the far-field. Reproduced with permission.<sup>[89]</sup> Copyright 2012, Macmillan Publishers. c) Sketch of LSPRs excitation in individual metallic nanoparticles. d) Examples of LSPR-based nanogaps in plasmonic materials. Reproduced with permission.<sup>[31]</sup> Copyright 2016, American Chemical Society. e) Mie-type resonances in high-refractive dielectrics. Electric (E) and magnetic (H) field distributions inside a high refractive index dielectric sphere at the magnetic resonance. Reproduced with permission.<sup>[90]</sup> f) Illustration of the electric and magnetic hotspots in silicon dimers. Reproduced with permission.<sup>[75]</sup> Copyright 2015, American Chemical Society. g) Illustration of the concept of bound states in the continuum (BICs) in comparison to other optical excitations. Reproduced with permission.<sup>[82]</sup> Copyright 2016, Macmillan Publishers. h) Examples of different meta-atoms used in symmetry-protected BIC metasurfaces. The radiative Q factor in such systems follows a characteristic inverse square law as a function of the asymmetry parameter. Reproduced with permission.<sup>[80]</sup> Copyright 2018, American Physical Society.

of metal nanoparticles such as dolmen structures,<sup>[47,48]</sup> oligomers,<sup>[49–51]</sup> and asymmetric resonators.<sup>[52,53]</sup> Recently, high refractive index dielectric materials with low loss have likewise been utilized for realizing resonances with reduced linewidth,<sup>[54,55]</sup> improving the spectral selectivity and thus positively affecting the achievable sensitivities.

## 2.2. Dielectrics

Nanostructured dielectric materials with high refractive index have emerged as a powerful toolkit for controlling light on the nanoscale,<sup>[56–61]</sup> and specifically for biosensing.<sup>[62–65]</sup> In contrast to plasmonic systems, where the optical response is dominated by electric multipoles,<sup>[22,66]</sup> resonances in dielectric particles readily support displacement currents driven by the incident light, allowing for the straightforward excitation of both electric and magnetic multipoles.<sup>[67–70]</sup> The resonant magnetic dipole response occurs when the wavelength of light inside the sphere becomes comparable to the sphere's diameter  $2R \approx \lambda/n$  ( $R$ : sphere radius,  $\lambda$ : light wavelength,  $n$ : refractive index of the sphere). Under this condition, the polarization of the electric field is anti-parallel at opposite boundaries of the sphere, leading to a coupling of incident light to circular displacement currents, which produces a magnetic field

perpendicular to the plane of the current loop (Figure 1e).<sup>[61,71]</sup> Both the electric and magnetic multipole modes can be tailored via the geometry of the dielectric resonators, unlocking a multitude of versatile nanophotonic designs.<sup>[59,72–74]</sup>

Combining both classes of modes, it has been demonstrated numerically and experimentally that a dimer of high refractive index dielectric nanoparticles with a nanometer-sized gap can simultaneously enhance the electric and magnetic field intensities by two orders of magnitude (Figure 1f).<sup>[75]</sup> The electric and magnetic hotspots at visible wavelengths can produce an increase of the local optical density of states (DOS), thus modifying the magnetic transition rates of molecules or emitters connected with an enhancement of the Purcell factor.<sup>[76,77]</sup> Because of these advantages, low loss dielectric systems are ideally suited for the detection of heat-sensitive biological species based on SEF and SERS while avoiding heat generation and transfer in the system.<sup>[78]</sup>

In the context of nanophotonic sensing, geometrically simple dielectric resonators such as spheres or disks are still limited by the confinement of the electromagnetic fields mostly to the interior of the structures, leading to low overlap with the target analytes, as well as by comparatively large resonance linewidths caused by radiative damping. To address these constraints, photonic BICs, which engineer the resonant coupling to the far-field to reduce radiative loss, have recently been proposed

and implemented in all-dielectric nanostructures including single nanoobjects<sup>[79]</sup> and metasurfaces.<sup>[80]</sup> Fundamentally, BICs lie within the radiation continuum, but with lifetimes and therefore  $Q$  factors approaching infinity, which is in contrast to the established understanding of resonances as leaky modes (Figure 1g).<sup>[81,82]</sup> Ideally, a true BIC with infinite  $Q$  factor can only occur in physical systems where at least one of the dimensions is infinite.<sup>[82]</sup> Practically, to exploit this phenomenon in all-dielectric nanophotonic platforms, different approaches for transforming BICs into quasi-BICs with finite  $Q$  factor have been explored, e.g., in the form of supercavity modes.<sup>[83]</sup> There are two popular groups of photonic quasi-BIC implementations: accidental BICs in single subwavelength dielectric resonators<sup>[79,84,85]</sup> and periodic arrays,<sup>[86]</sup> as well as symmetry-protected BICs in metasurfaces.<sup>[80]</sup> In general, accidental BICs emerge through the destructive interference of multiple resonant modes in nanophotonic structures, which can be achieved by continuous tuning of a system parameter. For example, in the case of individual dielectric resonators, this interference is realized by tuning the aspect ratio, whereas for periodic arrays such as photonic crystals, the tuning can be carried out via the incidence light angle. Likewise, the resonances of symmetry-protected BICs are controlled by the in-plane inversion symmetry of their constituent elements (i.e., meta-atoms), as shown in Figure 1h. The resulting radiative  $Q$  factor is closely correlated with the asymmetry parameter ( $\alpha$ ), following a characteristic inverse-square law.<sup>[80]</sup> The BIC concept can enable flexible tuning of the resonance frequency,  $Q$  factor, and surface-confined near-fields through careful design of geometry, orientation and arrangement of the constituent resonators, offering significant benefits for metasurface-based biochemical sensing.<sup>[63,87]</sup> Also, through a generalized scaling approach, a wide range of resonance frequencies can be realized from the visible to the infrared spectral regions,<sup>[80,88]</sup> facilitating the implementation of different optical transduction schemes.

In the following sections, we will highlight a broad range of nanophotonic sensing principles and discuss their physical mechanisms, including the refractometric monitoring of changes in the local environment, the emission of optical emitters, and the amplification of molecular vibrational signatures (surface-enhanced Raman and infrared spectroscopy). Furthermore, based on the respective strengths and weaknesses of the different metallic and dielectric transduction schemes, we will provide a perspective on relevant recent sensing applications for biomedical assays and clinical diagnostics.

### 3. Sensing Principles in Nanophotonics

Nanophotonics enables the efficient localization of light into nanoscale volumes comparable in size to many relevant biomolecules, strongly enhancing the light-matter interactions and transducing the molecular binding events into detectable far-field optical signals such as amplitude and phase changes, resonance frequency shifts, or fluorescence.<sup>[63,91,92]</sup> In addition, by targeting the characteristic molecular vibrations associated with the chemical bonds of molecules, surface-enhanced Raman spectroscopy (SERS) and surface-enhanced infrared absorption spectroscopy (SEIRAS) enable chemically specific

detection,<sup>[32,93,94]</sup> providing opportunities for realizing real-time studies of molecular binding dynamics and metabolic pathologies.<sup>[95,96]</sup> Building on these sensing principles, we will highlight how signal readouts can be amplified through specifically designed nanophotonic geometries with a particular focus on recently reported high-end biosensing applications, encompassing the detection of biomolecules (proteins, antigens, biomarkers), exosomes, pathogens (viruses and bacteria), and cell secretion.<sup>[97–100]</sup>

#### 3.1. Refractometry

The resonances produced by plasmonic nanomaterials, including single nanoparticles,<sup>[101,102]</sup> nanoapertures,<sup>[103,104]</sup> periodic nanohole arrays,<sup>[100,105,106]</sup> and metasurfaces<sup>[107]</sup> are highly sensitive to changes in the refractive index of the surrounding environment. Therefore, changes in surface mass caused by the attachment of analyte molecules onto the sensor surface can give rise to pronounced modulations of the resonance wavelength, amplitude, and phase (Figure 2a).<sup>[108–110]</sup> In the context of sensor miniaturization and on-chip integration, the use of LSPR-based platforms can often be advantageous due to the straightforward readout via far-field reflection/transmission measurements compared to the more complex optics required for SPR prism or grating coupling approaches. Therefore, LSPR-based biosensing concepts have been investigated intensely as a basis for fluidic integration, targeting high throughput real-time assays.<sup>[98]</sup> Despite these advances, the detection of single molecules has been a longstanding challenge for nanophotonic sensors, since individual molecules have to be precisely positioned in the near-field hotspots of the resonators in a controllable way and within the measurement time-frame. In addition, even though specific analyte detection can be achieved through surface functionalization, the strong molecular binding between the analyte and receptor often leads to a saturation of the hotspot binding sites, limiting sensor reuse and decreasing the throughput. To address these challenges, Shi et al. developed a LSPR-based biosensor for the active delivery of single molecules into a plasmonic nanopore with sub-millisecond acquisition rates by monitoring the back-scattered light intensity (Figure 2b).<sup>[111]</sup> A central advantage of this approach is the capability to actively drive molecules away from the hotspot by applying an electric field to the nanopore, preventing molecules from permanently binding to the sensor surface and allowing higher throughput detection. Furthermore, they demonstrated that DNA molecule translocation induced both a resonance redshift (on the timescales of tens of milliseconds) and a scattered light intensity change at a fixed excitation wavelength (in microseconds), based on the refractive index variations associated with molecular binding on the sensor surface. This technique was shown to outperform other methods such as dark-field spectroscopy,<sup>[112]</sup> single nanorod scattering,<sup>[113]</sup> and double nanohole trapping<sup>[114]</sup> in terms of time resolution, waiting time and maximum number of detection events.

As a prominent example of array-based plasmonic sensors, plasmonic nanohole arrays (NHAs) leverage the coupling between localized resonances and extended non-radiative

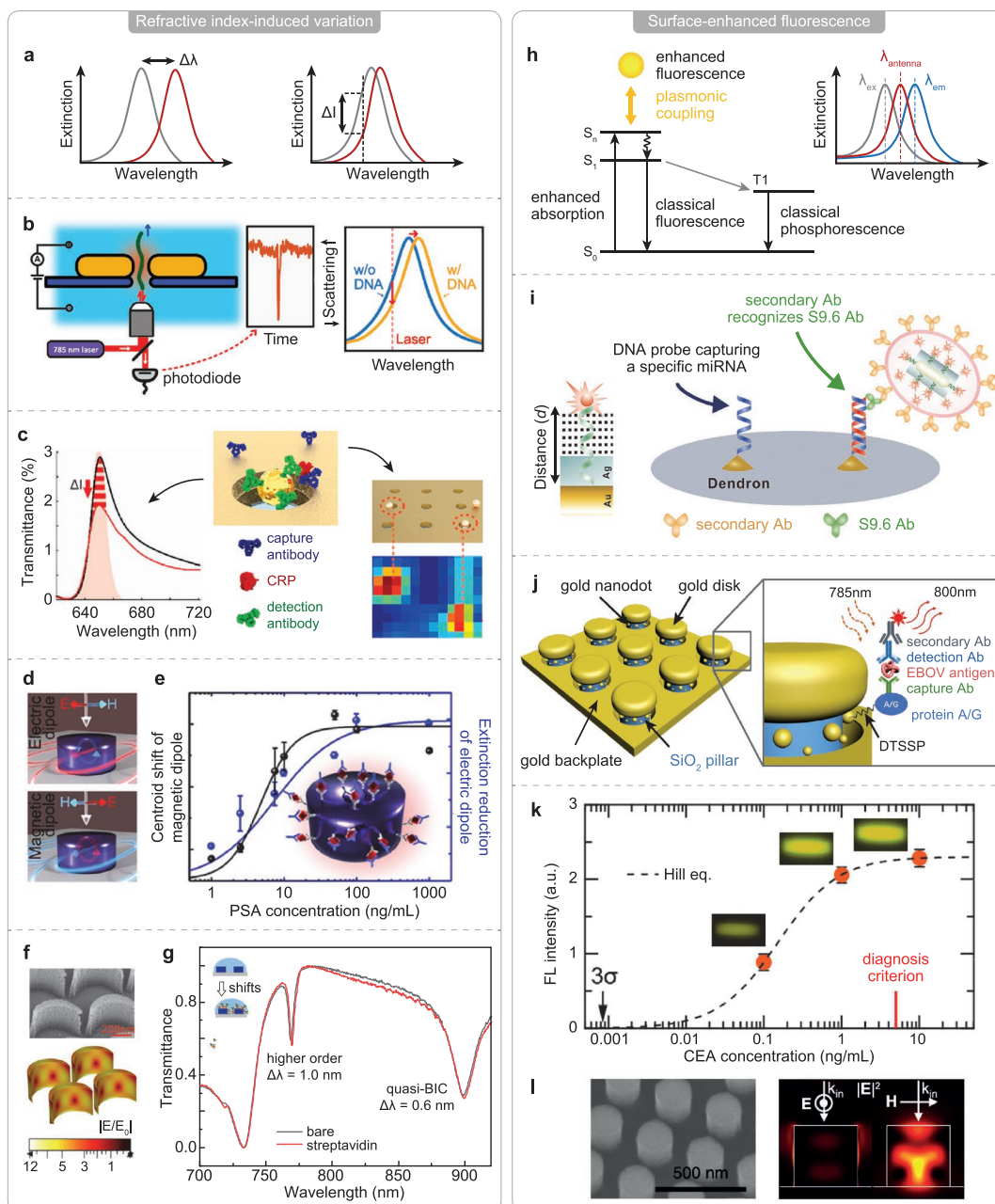


**Figure 2.** Refractometric detection and surface-enhanced fluorescence sensing. a) Schematic of refractive index-induced changes of the optical response upon molecular binding on the sensor surface. b) Active delivery of DNA molecules into a plasmonic nanopore for optical sensing. Reproduced with permission.<sup>[111]</sup> Copyright 2018, American Chemical Society. c) Au nanoparticle-enhanced plasmonic biosensor for the digital detection of C-reactive protein (CRP) biomarker. Reproduced with permission.<sup>[92]</sup> Copyright 2018, American Chemical Society. d) Schematic of the electric and magnetic dipoles in a Si disk resonator. e) Resonance shift and extinction reduction as a function of the target PSA concentration. Reproduced with permission.<sup>[91]</sup> Copyright 2019, American Chemical Society. f) Close-up scanning electron microscope (SEM) image and near-field distribution of a crescent metasurface supporting quasi-BICs and higher-order resonances for biomolecular detection. g) Optical signal response of the crescent metasurface upon streptavidin protein binding from buffer solution. Reproduced with permission.<sup>[88]</sup> Copyright 2021, American Chemical Society. h) Principle of SEF. i) Ultraflat faceted nanocuboids enable enhanced fluorescence signals for microRNA detection. Reproduced with permission.<sup>[140]</sup> Copyright 2021, American Chemical Society. j) 3D plasmonic nanoantenna arrays for Ebola virus antigen sensing. Reproduced with permission.<sup>[141]</sup> Copyright 2019, Wiley. k) All-dielectric metasurface for fluorescence-based antibody/antigen detection. Fluorescence intensity as a function of target concentration. l) Close-up SEM image and simulated near-field distribution in the Si disks. Reproduced with permission.<sup>[142]</sup> Copyright 2020, American Chemical Society.

modes associated with the grating to reduce the radiative losses down to the limit of metal-intrinsic Ohmic damping.<sup>[115]</sup> The resulting Fano resonances in the NHAs combine high surface

sensitivity and comparatively sharp resonances for efficient sensing. Furthermore, since NHAs exhibit high transmission at resonance (extraordinary optical transmission, EOT) while

suppressing it in other spectral ranges, they can be applied for spectrometer-less detection by simply monitoring the transmittance changes near the resonance (e.g., using a low-cost light-emitting diode and a camera), taking an important step toward practical POC devices.<sup>[105]</sup> In experiments, the spatially resolved transmitted intensity<sup>[100]</sup> could be mapped using a narrowband illumination source together with a charge-coupled device (CCD) or complementary metal-oxide-semiconductor (CMOS) imager. Through careful design of the nanohole periodicity, the enhanced near-field space can be tuned to overlap with the dimensions of the analytes of interest, maximizing the sensitivity.<sup>[100]</sup> Moreover, through coupling of gold nanoparticles with the NHAs,<sup>[92]</sup> the sensitivity can be further boosted (Figure 2c), showing an impressive enhancement of three orders of magnitude compared to the basic nanohole configuration.<sup>[105]</sup>

Even though plasmonic biosensors can achieve competitive detection limits and straightforward integration for POC devices,<sup>[111]</sup> they often require intense illumination to obtain the high signal-to-noise ratios required for single molecule detection. Consequently, intrinsic absorption losses may cause photothermal degradation of the analyte or the sensor itself.<sup>[19]</sup> Here, all-dielectric sensors incorporating high refractive index resonators are a promising alternative to plasmonics because of their negligible absorption losses over a broad spectral range and their capability of transducing refractive index changes in the local environment into modulations of their far-field optical response.<sup>[55,116]</sup> Widely used working principles of dielectric resonators include Mie-type scattering,<sup>[117]</sup> lattice resonances<sup>[21]</sup> and quasi-BICs.<sup>[55,88]</sup> Through careful nanophotonic design, such dielectric sensors have already shown comparable sensing capabilities to their LSPR counterparts. For example, Yavas et al. found that the electric and magnetic dipole resonances in silicon disks are correlated with a decrease of the extinction and a shift of the resonance, respectively (Figure 2d). The limit of detection of prostate specific antigen (PSA) protein cancer biomarker evaluated by extinction reduction was shown to be 0.83 ng mL<sup>-1</sup>, outperforming the analysis based on resonance shift with 1.55 ng mL<sup>-1</sup> (Figure 2e). Such mode-determined detection responses can be explained by the higher exposure of the electric fields to the surrounding medium, whereas the magnetic dipole modes are highly confined inside the resonator volume, leading to smaller sensitivity to changes at the surface. Moreover, many biologically and medically relevant real-time bioassays are conducted in fluidic buffer environments, which decreases the refractive index contrast between the surface bonded/adsorbed molecules and the dielectric environment compared to measurements in air, reducing the achievable sensitivity.<sup>[118]</sup> To address this issue, higher-order resonances in BIC-inspired metasurfaces (Figure 2f) have been shown to provide higher spectral resolution and sensing performance than the fundamental modes for detection in solution, as demonstrated by Wang et al.,<sup>[88]</sup> (Figure 2g) and Shi et al.,<sup>[119]</sup> indicating a clear advantage of employing such higher-order resonances for biosensing.

Another important aspect for biosensing in realistic systems is the discrimination of enantiomers, which have identical molecular formulas but are mirror images of each other in terms of molecular structure. This class of molecules plays a crucial role for protein function, cell communication and

organism health,<sup>[120,121]</sup> because different enantiomers can have markedly different biological and pharmacological functions.<sup>[122]</sup> Circular dichroism (CD) spectroscopy can be used to resolve enantiomeric properties, but struggles for trace amounts of such chiral molecules,<sup>[123]</sup> creating opportunities for leveraging nanophotonic enhancement in chiral sensing.<sup>[124–129]</sup> Recent examples span the gamut from twisted plasmonic metasurfaces with detection limits approaching the zeptomole level<sup>[130]</sup> to sensing platforms for resolving the composition of chiral mixtures using all-dielectric BIC-based metasurfaces,<sup>[87]</sup> highlighting the potential for further optofluidic integration to enable real-time and in-situ operation.

### 3.2. Surface-Enhanced Fluorescence Sensing

Enhanced near-fields around nanophotonic structures can directly affect the electronic transitions and consequently the emission properties of optical emitters in close proximity.<sup>[131–133]</sup> To date, metallic structures have been widely investigated for fluorescence-based sensing with the goal of achieving improved sensitivity and lower detection limit. However, in such metallic geometries, one has to carefully control the separation between the resonator surface and the emitters, since quenching of the fluorophore emission can occur for distances below  $\approx 5$  nm.<sup>[134]</sup> Many efforts have been made to tailor nanophotonic platforms to enable the simultaneous enhancement of fluorophore excitation and emission by tuning the resonance frequency of the resonators (Figure 2h), while maintaining strong near-field enhancements.<sup>[135–137]</sup> Similarly, precise tailoring of the fluorophore-resonator distance can be achieved by using assembly techniques such as polymer brush growth.<sup>[138,139]</sup> Due to low fabrication costs, multiplexing capability and the ability to work with low sample volumes, SEF techniques have been applied in biosensing toward clinical and POC tests. Here, Cruz et al. reported a sandwich immunoassay microarray consisting of plasmonic nanogap cavities for the detection of the cardiac biomarker B-type natriuretic peptide with a detection limit of 0.02 ng mL<sup>-1</sup>, which shows a 151-fold increase in fluorescence and 19-fold improvement in detection limit compared to the unenhanced assay.<sup>[139]</sup> However, maximizing fluorescence enhancement for biomolecular quantification is highly challenging, because even small variations of fluorophore separation from the plasmonic resonators can cause significant changes of the fluorescence signal. To address this limitation, Hwang et al. designed a microarray-based microRNA sensor consisting of fluorescence-amplified nanocuboids with highly controlled plasmon-enhanced fluorescence (Figure 2i), achieving more than 1000-fold higher sensitivity than that of commercially available chemical fluorophores with a dynamic range from  $100 \times 10^{-18}$  M to  $1 \times 10^{-12}$  M.<sup>[140]</sup> Here, reliable control over the distance between the fluorophores and the silver surface is realized by uniform modification of fluorescently labeled DNA on gold nanorods combined with the subsequent formation of ultraflat silver and silica shells, which can fix fluorophore dye positions inside the shell and minimize the fluorescence signal fluctuation.

Targeting the mounting global challenges associated with infectious diseases, ultrasensitive detection of pathogens has

been demonstrated using a 3D plasmonic sensor device consisting of a SiO<sub>2</sub> nanopillar array with a gold nanodisk placed on top of each pillar, gold nanodots on the pillar walls, and a gold backplane (Figure 2j).<sup>[141]</sup> Through a sandwich assay protocol, this 3D nanoantenna sensor achieved quantification of Ebola virus (EBOV) soluble glycoprotein (s-GP) in human plasma down to 220 fg mL<sup>-1</sup>, indicating a more than four orders of magnitude higher sensitivity than existing rapid EBOV immunoassays. Furthermore, the authors demonstrated that the sensor could detect sGP-spiked human plasma samples at two times the limit of detection with comparable sensitivity. The improvements in sensitivity and detection limit are attributed to the i) plasmonic nanocavity array formed by the gold disks and gold backplane, maximizing excitation laser absorption and emission of emitters, and ii) nanodots with enhanced localized near-fields for further light-emitter enhancement, resulting in a substantial increase of fluorescence signal emission from the emitters. It is worth noting that the pre-functionalized self-assembled monolayer (SAM) and the capture antibody serve as a spacer with the thickness of about 6.1 nm to prevent nonradiative fluorescence signal loss associated with the gold surfaces.

Ohmic losses and quenching effects predominantly occur in metallic structures. In contrast, the use of low-loss high refractive index materials can avoid these negative influences when excitation takes places at wavelengths above their bandgap.<sup>[143]</sup> Also, since the distance of the emitters to the resonators no longer has to be carefully controlled, additional design degrees of freedom for fluorescence-based sensing are unlocked. When placing the fluorophores within the nanogaps of dielectric dimers made of Si or gallium phosphide (GaP), fluorescence enhancement factors (EFs) ranging from 250 to 3600 can be achieved, driven by the strong near-field enhancement.<sup>[143,144]</sup> All-dielectric metasurfaces have also been applied for biomolecular detection using enhanced fluorescence.<sup>[142]</sup> For example, Iwanaga et al. demonstrated the detection of antibodies and antigens with high sensitivity and improved detection limit using an all-dielectric silicon metasurface together with a sandwich assay protocol.<sup>[142]</sup> They found that the electric field intensity has a maximum at the outermost surface of the resonators (Figure 2l), leading to highly enhanced fluorescence. In addition, carcinoembryonic antigen (CEA) detection was successfully performed well below the clinical diagnostic level of 5 ng mL<sup>-1</sup> and reached a detection limit of 0.85 pg mL<sup>-1</sup> (Figure 2k). In comparison with conventional ELISA, this sensing platform offers better sensitivity and higher throughput with detection times of less than 90 min.

Romano et al. demonstrated an ultrasensitive refractive index imaging method to monitor the spatially varying surface refractive index of living cells cultured on an all-dielectric photonic crystal slab (PhCS), leveraging both SEF and refractometric sensing based on the underlying photonic quasi-BICs.<sup>[63]</sup> The enhanced near-fields of the first resonance were shown to amplify the emitter emission by two orders of magnitude. Simultaneously, hyperspectral refractometric sensing was used to map the spatially varying refractive index produced by the specimen on the PhCS, utilizing Fano interference between the second mode and the fluorescence emission. This dual sensing mechanism enables a correlative imaging platform that can be

applied in many fields such as surface cell analysis, molecular interactions, and chemical reactions.

Even though refractometry and SEF-based sensing can efficiently transduce molecular surface-binding events and are able to achieve multiplexed assays with high throughput, they still face limitations to spatially and temporally resolve the full chemically specific information associated with biomolecular surface binding. Surface-enhanced vibrational spectroscopy can help to fill this gap, providing unique opportunities to study protein configuration, perform drug screening, and unravel metabolic processes.<sup>[145]</sup>

### 3.3. Surface-Enhanced Vibrational Spectroscopy

Ultrasensitive molecular spectroscopy and real-time dynamic monitoring are of paramount importance for biomedical assays, clinical diagnostics, as well as for material and environmental science. However, due to the extremely low absorption cross-sections of the target molecules, either large amounts of analytes or high-powered laser sources are often required, which increase the technological complexity, can degrade the molecules, and limit the detection of trace amounts of analytes. To overcome these constraints, surface-enhanced vibrational spectroscopic techniques have been introduced, in particular SERS and SEIRAS, which rely on the amplification of molecular vibrations through contact with nanostructured surfaces (Figure 3a,e).<sup>[32,146]</sup> In this section, we discuss the use of these surface-enhanced techniques for molecular identification,<sup>[147–149]</sup> with a particular focus on recently introduced strategies toward the ultimate goal of performing diagnostically relevant biosays in bodily fluids.

#### 3.3.1. Surface-Enhanced Raman Spectroscopy

Two of the most popular strategies for SERS are the indirect label-mediated<sup>[150]</sup> and direct label-free approaches.<sup>[151,152]</sup> In label-mediated SERS, the detection of molecules of interests is carried out indirectly through pre-functionalized SERS tag molecules that are specifically designed to track the target analyte molecules for differentiation and quantification. In contrast, label-free SERS approaches measure the Raman signals of the molecules of interest directly, allowing for real-time monitoring in a contactless, non-invasive and non-destructive manner, especially in biological systems.<sup>[153,154]</sup> Because molecular signal enhancement occurs only within a small region a few nanometers away from the resonator surface, developing a clear understanding of the biochemical composition in a complex 3D biological sample is crucial to avoid experimental bias or false interpretations in the resulting SERS spectra. For example, the refractive index distribution in a cell culture is highly heterogeneous within a range of 1.30 to 1.60.<sup>[155]</sup> Also, because the local refractive index directly influences the SERS EFs, the refractive index variation of the surroundings can negatively impact the reliable spatiotemporal SERS analysis of living cells with different extra/intracellular organelles. To resolve this issue, Nam et al. designed a refractive index insensitive nanolaminated SERS substrate with uniform arrays of

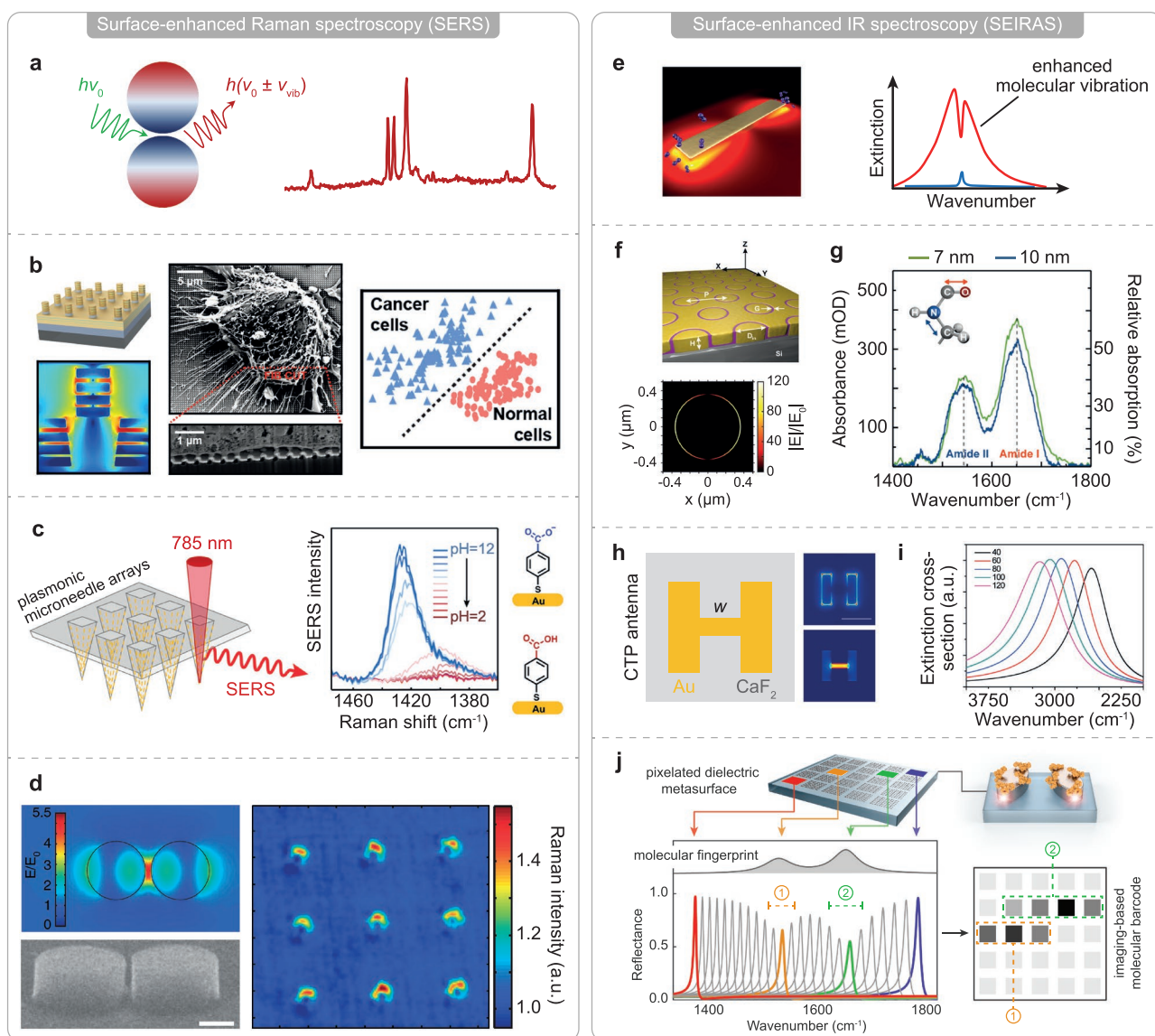


**Figure 3.** Surface-enhanced vibrational spectroscopy. a) Schematic of LSPR-based SERS. b) A refractive index insensitive nanolaminated SERS substrate for label-free Raman profiling and living cancer cells classification. Cross-sectional SEM image of the substrate and associated near-field enhancement. Reproduced with permission.<sup>[153]</sup> Copyright 2019, American Chemical Society. c) In-situ sensing of pH in human skin by a plasmonic microneedle array. Schematic of the plasmonic microneedle array and the corresponding SERS activity. Reproduced with permission.<sup>[158]</sup> Copyright 2019, American Chemical Society. d) Dimer-like silicon-based single nanoantennas for SERS with a negligible temperature increase in their hotspots and surroundings. Reproduced with permission.<sup>[78]</sup> Copyright 2015, Macmillan Publishers Limited. e) Principle of SEIRAS-enabled nanophotonic platforms. Reproduced with permission.<sup>[165]</sup> Copyright 2017, American Chemical Society. f) Resonant coaxial nanoapertures for SEIRA-based molecular detection. Schematic of a nanoaperture array on a Si substrate and horizontal electric field distribution. g) Influence of the coaxial nanoaperture gap size on the analyte absorption intensity. Reproduced with permission.<sup>[175]</sup> Copyright 2018, American Chemical Society. Demonstration of CTP enabled tunability of the resonances in a wide IR range with nanometer-scale variation. h) Schematic of the CTP antenna and its corresponding near-fields distribution. i) Extinction spectra of this CTP-based antenna as a function of the conductive bridge width. Reproduced with permission.<sup>[189]</sup> Copyright 2019, American Chemical Society. j) Imaging-based molecular barcoding by pixelated all-dielectric high-Q metasurfaces. Reproduced with permission.<sup>[179]</sup> Copyright 2018, American Association for the Advancement of Science.

vertically oriented nanogap hotspots with large SERS EFs of  $10^7$  (Figure 3b).<sup>[153]</sup> They have successfully demonstrated label-free SERS measurements and analyzed living breast cancer and breast normal cells with the assistance of multivariate analysis (Figure 3b), including principal component analysis (PCA) and a predictive classification model constructed by supervised linear discriminant analysis (LDA). Such a refractive index

insensitive SERS-active substrate provides a broadband optical response supporting multiple plasmonic modes concentrated in nanogap hotspots over a wide wavelength range at different refractive index surroundings (Figure 3b).

Another prominent example is the integration of nanophotonic platforms with microneedles for diagnostics based on interstitial fluid (ISF), which is rich in biomarkers.<sup>[156]</sup> In



order to efficiently capture the target biomarkers from the ISF, such arrays can be combined with chemical surface functionalization.<sup>[157]</sup> For instance, Park et al. reported the integration of SERS-active units with a microneedle array fabricated from a commercial polymeric adhesive and coated with plasmonic gold nanorods that were functionalized with pH-sensitive molecules, allowing to monitor pH over a range from 5 to 9 and to detect pH levels in human skin in-situ (Figure 3c). Such microneedle arrays with high flexibility and minimally invasive collection and in-situ analysis of biomarkers from ISF could pave the way toward POC diagnostics for resource-limited settings and continuous monitoring.<sup>[157,158]</sup>

Nanoscale heating in plasmonic structures can lead to the vaporization of the surrounding solvent media,<sup>[159]</sup> modifying the properties of emitters, molecules, and tissues close to them and causing the retrieval of inaccurate SERS signals.<sup>[160]</sup> Similar to the refractometric approaches discussed above, all-dielectric resonators with low loss are an ideal alternative for use in temperature-sensitive systems. For example, Caldarola et al. have demonstrated silicon dimers for Raman signal enhancement, which generate a negligible temperature increase in their hot-spots and local environment (Figure 3d).<sup>[78,161,162]</sup>

Currently achievable Raman enhancement factors of all-dielectric platforms are still below the values obtained from plasmonic structures. However, the versatile resonance control afforded by dielectric systems provides many opportunities to further engineer the near-fields and amplify the vibrational signals, for example by utilizing higher order electric and magnetic modes or by exploring alternative materials such as TiO<sub>2</sub>,<sup>[163]</sup> enabling real-time bioassays without associated heating issues.<sup>[154]</sup>

### 3.3.2. Surface-Enhanced Infrared Absorption Spectroscopy (SEIRAS)

Infrared (IR) spectroscopy complements Raman spectroscopy by targeting additional vibrational bands and has similarly been used for molecular identification in a non-destructive and non-invasive way without the use of additional labels. Despite these advantages, traditional far-field IR techniques (e.g., cuvette-based transmission measurements) still face sensitivity challenges due to the pronounced mismatch between the size of the target molecules on the order of nanometers and the mid-IR wavelengths on the order of microns, which can be addressed through nanophotonic light confinement (Figure 3e). Since the first experimental demonstration of thin metal films for SEIRA spectroscopy,<sup>[164]</sup> research into SEIRAS platform has grown enormously. In contrast to SERS geometries operating at visible wavelengths, where the strong field confinement facilitates the detection of very small molecules, SEIRAS with larger decay length can resolve molecules with more than a few nanometers in size, particularly proteins, bacteria, and cells, facilitating detection in complex biological systems like organ-on-chip platforms.<sup>[96]</sup> Significant efforts have been made to engineer a variety of resonators with enhanced near-fields and controllable resonant frequency,<sup>[165]</sup> including metallic nanorods/nanoslits,<sup>[166]</sup> nano-gapped antennas,<sup>[33,167]</sup> split-ring resonators,<sup>[168]</sup> fan-shaped nanoantennas,<sup>[169]</sup>

nanoantennas on nanopedestals,<sup>[170,171]</sup> and metamaterial perfect absorbers (MPAs).<sup>[172,173]</sup> These SEIRA-based nanophotonic platforms have realized EFs of 10<sup>4</sup>–10<sup>7</sup><sup>[166,174]</sup> for biomolecular detection, enabled by the coupling between the enhanced near-fields of the resonators and the vibrational modes of the target molecules. In the following, we will highlight several recent nanophotonic SEIRA platforms with great potential for fluidic integration toward real-time optofluidic sensing, focusing on Fabry-Pérot (FP) optical cavities,<sup>[175,176]</sup> MPAs,<sup>[177,178]</sup> and all-dielectric metasurfaces based on photonic quasi-BICs.<sup>[179,180]</sup>

Conceptually, a coaxial aperture with a diameter on the order of micrometers and a sub-10 nm gap can be designed to support a zeroth order FP resonance in the mid-IR region,<sup>[181]</sup> where the incident light couples into ultranarrow annular nanogaps (Figure 3f). The aperture supports strong near-field enhancements and EOT resonances in the far-field spectra, making this configuration highly effective for resonant SEIRAS.<sup>[175]</sup> Notably, the resonance frequency of the zeroth order mode is mainly determined by the geometry of the aperture (inner diameter and gap size) instead of the periodicity of the array, which unlocks additional resonance engineering.<sup>[7,182]</sup> The created hot-spots also serve as channels to trap and confine the analytes, which can improve the detection limit (Figure 3g).

MPAs<sup>[183,184]</sup> consist of a periodic array of plasmonic nano-antenna on top of a metallic mirror and separated by a thin dielectric spacer layer, which results in strongly enhanced near-fields in the resulting cavities and near-unity absorption.<sup>[185–187]</sup> By combining a plasmonic MPA chip with tetrahedral DNA nanostructures, Hui et al. have demonstrated ultrasensitive quantification of microRNA molecules with very high sensitivity and an extremely low detection limit of 0.1 × 10<sup>-12</sup> M, which is about 100 times lower than that of previously used fluorescence-based detection methods.<sup>[177]</sup> Importantly, to achieve compact and portable diagnostic devices, there is a need for reducing the size of the nanoantennas while simultaneously targeting vibrational bands in a wide spectral range, which requires methods for precisely tuning the antenna resonances through nanometer-scale size vibration. Using Fabry-Pérot modes in nanostructured metal-insulator-metal (MIM) resonators, Yoo et al. showed that the resonances could be readily tailored within sub-10 nm insulator gaps for SEIRA through atomic layer lithography.<sup>[181]</sup> However, the realization of resonances over a wide spectral range is still challenging for many plasmonic systems, due to the large geometry variations required for broad spectral detuning. Here, charge transfer plasmon (CTP) modes (Figure 3h)<sup>[188]</sup> are an intriguing approach for realizing controllable resonances for SEIRA, since they utilize the variation of the width of a conductive bridge instead of tuning the size of a sub-nm gap.<sup>[189]</sup> The CTP method enables 600 cm<sup>-1</sup> spectral shifts via changing the width of the bridge on the nanometer scale (Figure 3i), which cannot be achieved by, e.g., conventional bar-shaped dipole antennas.

Even though plasmonic structures have achieved SEIRA measurements with high EFs of more than 10<sup>3</sup> in the mid-IR spectral region, they are still subject to Ohmic losses with associated broad resonances, often much broader than the target molecular vibration bands of interest, limiting their spectral selectivity. To address this issue, Tittel et al. have proposed a pixelated all-dielectric metasurface with ultrasharp resonances for

imaging-based molecular detection.<sup>[179]</sup> The metasurface consists of a pair of tilted silicon ellipses arranged in a periodic array, working within the framework of quasi-BICs (Figure 3j). A significant advantage of this approach is the straightforward resonance tuning over a broad spectral range via geometrical scaling, targeting the mid-IR fingerprint range from 800 to 4000  $\text{cm}^{-1}$  while maintaining  $Q$  factors above 100. This functionality leads to improved spectral selectivity combined with high sensitivity for applications in biosensing, materials science, and environmental monitoring. Furthermore, Leitis et al. have utilized the incident angle of mid-IR light to tune highly surface-sensitive and spectrally sharp resonances from a single BIC-based metasurface for protein detection.<sup>[180]</sup> Such high- $Q$  nanophotonic platforms hold great potential for developing POC sensing devices, since molecular fingerprint information can be retrieved with broadband light sources and detectors, allowing for spectrometer-less operation.

In summary, we have discussed how SPR-based platforms can provide high sensitivity and have shown great potential for diagnostic applications, but still face limitations related to high throughput assays and sensor miniaturization. On the other hand, LSPR-based nanophotonic approaches excel at multiplexed and parallel assays while enabling straightforward on-chip integration toward POC devices and clinical diagnostics. However, they often still exhibit lower sensitivities compared to surface-enhanced fluorescence and vibrational spectroscopy techniques. Recently introduced all-dielectric nanophotonic platforms can overcome the constraints of low resonance  $Q$  factors and heat generation, promising higher sensitivities and improved operation in heat-sensitive biological systems. Nevertheless, there is significant room to improve the performance of such dielectric structures for practical sensing applications, for example by tailoring the spatial near-field overlap with bonded molecules.

## 4. Fluidic Engineering

Advances in nanotechnology and fluidics have enabled unique perspectives for controlling analyte flow in micro- and nanoscale volumes.<sup>[190,191]</sup> For analyte systems with ultralow concentrations, engineering such fluidic effects has become crucial for optimizing the surface binding efficiency. To date, a large amount of research has focused on the realization of compact nanophotonic devices with small footprints on micrometer or even nanometer length scales for POC devices. Therefore, it is crucial to understand the background and mechanisms of fluidic behavior and manipulation in ultrasmall volumes as well as how to combine such fluidics with nanophotonic signal transducers. In the following, we will discuss some critical aspects for integrating micro/nanofluidic compartments into nanophotonic platforms (Figure 4) and provide perspectives for real-world biosensing applications.

### 4.1. Chip Bonding

To create channels within a sealed fluidic cell, one of the most popular materials used is dimethylpolysiloxane (PDMS), due to

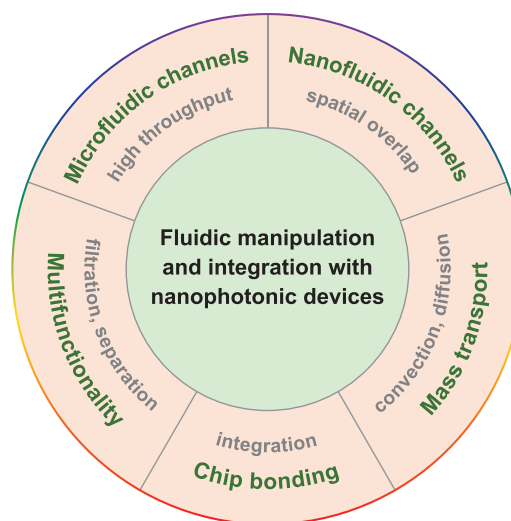


**Figure 4.** Aspects of micro/nanofluidic integration with nanophotonic platforms.

its ease of fabrication and biocompatibility. However, precisely engineering nanometric structures in such a soft material can prove challenging because of its deformability. Even though hard wafer materials including fused silica and silicon can help address this issue, they have poor compatibility with nanostructured plasmonic and dielectric materials. Generally, these hard wafer materials are subjected to the high temperatures (around 1000°C for fused silica glass) and harsh chemical treatments (e.g., acidic solution) associated with the required chip bonding process, which is the most crucial step in the fabrication of fluidic chips. With the aid of low-temperature bonding techniques such as plasma-based surface activation<sup>[192]</sup> and  $\text{O}_3$  activation,<sup>[193]</sup> fused silica glass (with high transmission in the visible and near-IR range) and  $\text{CaF}_2$  (with high transmission in the mid-IR range) have been used to realize nanofluidic channels on optical chips. However, the bonding strength and interface were found to still not be strong enough to withstand the influence of water stress for continuous long-term sensing of analyte dynamics.<sup>[194]</sup> In particular, conventional transparent IR materials (such as  $\text{CaF}_2$ ,  $\text{MgF}_2$ ) are not stable under established chemical surface treatment processes, and it therefore becomes critically important to develop new strategies for bonding transparent IR materials with nanophotonic chips. Toward this end, Xu et al. have developed a self-driven sapphire ( $\text{Al}_2\text{O}_3$ )-based mid-IR hybrid nanofluidic-SEIRAS platform for liquid sensors, where they exploited the plasma activation method for direct bonding of  $\text{Al}_2\text{O}_3$  with  $\text{SiO}_2$  at low temperature.<sup>[195]</sup> Also, engineering of metamaterials on ultrathin metal oxides and dielectric membranes can be an alternative approach instead of fabricating on hard transparent substrates, because the ultrathin metal oxides and membranes can also provide a wide range of useable transmission windows.<sup>[196]</sup>

### 4.2. Micro- and Nanofluidic Manipulation

One of the key advantages of integrating microfluidic channels onto nanophotonic sensor chips is to enable parallelized

multiplexed assays with high throughput. Compared to traditional ELISA approaches, such integrated platforms can make the detection of local surface-binding events much more time-efficient and reliable.<sup>[10,197,198]</sup> Recently, this concept has been extended toward modular microfluidic devices through the realization of a standardized plug-and-play fluidic circuit board (FCB) for operating multiple microfluidic building blocks (MFBBs).<sup>[197]</sup> A single FCB can parallelize up to three MFBBs of the same design or operate MFBBs with entirely different architectures, whereby the operation of MFBBs through the FCB is fully automated and does not require additional external footprint. This provides increased flexibility for integrating the nanophotonic sensors with different configurations. In particular, such microfluidic units have been demonstrated for on-chip cell cultures,<sup>[199]</sup> highlighting the potential of this method for the real-time monitoring of single cells.<sup>[145]</sup>

Besides the multiplexed and parallelized assays enabled by independently controlled microfluidic channels, control over fluids in nanofluidic channels also plays an important role, since the light-matter interactions can only be maximized and fully exploited when the fluidic analytes are precisely confined to the nanoscale hotspots. As a result, this approach provides opportunities to achieve single molecule sensing with greatly decreased background noise. For example, on-chip referenced single particle nanoplasmonic sensing in individual nanochannels has been reported,<sup>[200]</sup> which makes it possible to probe the entire nanovolume of fluids flowing past the antenna. Also, by leveraging the nanophotonic configuration itself, such as with a MIM structure as discussed above, transduction and amplification can be realized in a hybrid nanofluidic-nanophotonic device.<sup>[195]</sup>

Micro/nanofluidics are not only capable of manipulating fluids, but can also couple to functional modules for realizing lab-on-a-chip and organ-on-a-chip systems.<sup>[199,201]</sup> Based on these technologies, effective sample treatment can be accomplished on chip, including purification, separation, and concentration,<sup>[202]</sup> which is highly desirable for real-world applications and especially when targeting analytes in bodily fluids. This approach allows to purify/extract/concentrate molecules of interests in a sample before it reaches the nanophotonic sensor module, enabling on-chip sensing toward high-end POC devices.

### 4.3. Mass Transport

Convective flow, diffusion and chemical reactions of analytes are crucial aspects for surface binding events.<sup>[203–205]</sup> Here, the acceleration of molecular binding into nanophotonic hotspots is a central point, especially for ultralow concentrations of analytes. Squires et al. have developed a physical understanding of how the sensor dimensions (including the length, width and height as well as the fluidic channel dimensions) affect analyte delivery, providing insights on analyte transport in surface-based sensing systems.<sup>[204,206]</sup> Moreover, Sheehan et al.<sup>[207]</sup> have demonstrated that the realization of ultralow molecular detection limits is constrained by analyte transport rather than by the transduction performance offered by nanophotonic platforms. Therefore, to break this diffusion limit, active control

methods such as electrophoretic fields<sup>[15,208]</sup> and external magnetic force<sup>[209]</sup> have been demonstrated. Another approach is to increase the convection of analytes, which can also increase the total flux of analytes binding to the sensor.<sup>[206]</sup> As an alternative, a flow-through sensor format has been designed to increase the flux by directing the analytes directly through a nanohole array sensor, offering up to two orders of magnitude more diffusive flux of analytes to the sensor surface in comparison with a flow-over sensor, with the same sensing surface area and volumetric flow rate.<sup>[210]</sup> Also, the flow-through sensor can provide 20-fold faster time response for small and rapidly diffusing analyte molecules with relatively fast reaction kinetics.

Additionally, the shape of the individual resonators has a strong influence on the sensitivity, due to the differences in molecule accumulation on the sensor surface over a fixed time scale.<sup>[207]</sup> For example, the accumulation of analyte molecules on a cylindrical wire sensor was shown to increase linearly with increasing length instead of radius, whereas for a disk-shaped sensor, the increase was mostly correlated with the radius. Also, the configuration of the optical sensors (e.g., single particle, periodic array, radial array) and their surface area have a strong influence on the mass transport to the sensor surface.<sup>[205,211]</sup> These aspects require careful consideration of the shape of the building blocks, the configuration, and the surface area of the sensor, especially when pushing toward the detection of analytes with ultralow concentration.

## 5. Progress in Optofluidic Biosensors

Based on the fundamental aspects of nanophotonics and fluidic integration introduced before, we will now provide some examples to highlight the unique capabilities of optofluidic sensors for advanced bioassays and their applications in POC devices and resource-limited settings. For instance, Quidant et al. have demonstrated on-chip biosensing based on both plasmonic LSPR resonators<sup>[20]</sup> and all-dielectric nanoresonators,<sup>[21]</sup> leveraging multiple optofluidic channels on one chip that can be controlled independently and simultaneously through micro-mechanical valves (**Figure 5a**). The micromechanical valves<sup>[212]</sup> are thin PDMS membranes between the flow layer and the control layer of the chip, which can be precisely controlled through external pressure, enabling automatic and high throughput assays in a state-of-the-art microfluidic chip. Through a sandwich assay combined with a periodic array of silicon disks, they demonstrated that the resulting platform was suitable for the detection of small biomolecules in complex matrixes for clinical diagnosis, providing opportunities for the development of POC devices toward personalized healthcare. Furthermore, they showed sensing of the prostate specific antigen (PSA) cancer biomarker with a dynamic range from 2.5 to 16.0 ng mL<sup>-1</sup> and a limit of detection down to 1.6 ng mL<sup>-1</sup>, below the clinical cut-off value of the PSA concentration in patient samples (**Figure 5b**).

To accelerate the analyte transport and optimally leverage the nanophotonic hotspots, Wang et al. demonstrated a lateral flow-through biosensor consisting of a periodic array of silicon nanodisks on a silicon-on-insulator (SOI) substrate,<sup>[5]</sup> in which the PDMS slab was directly bonded onto the metasurfaces (**Figure 5c**), restricting the flow to the space between

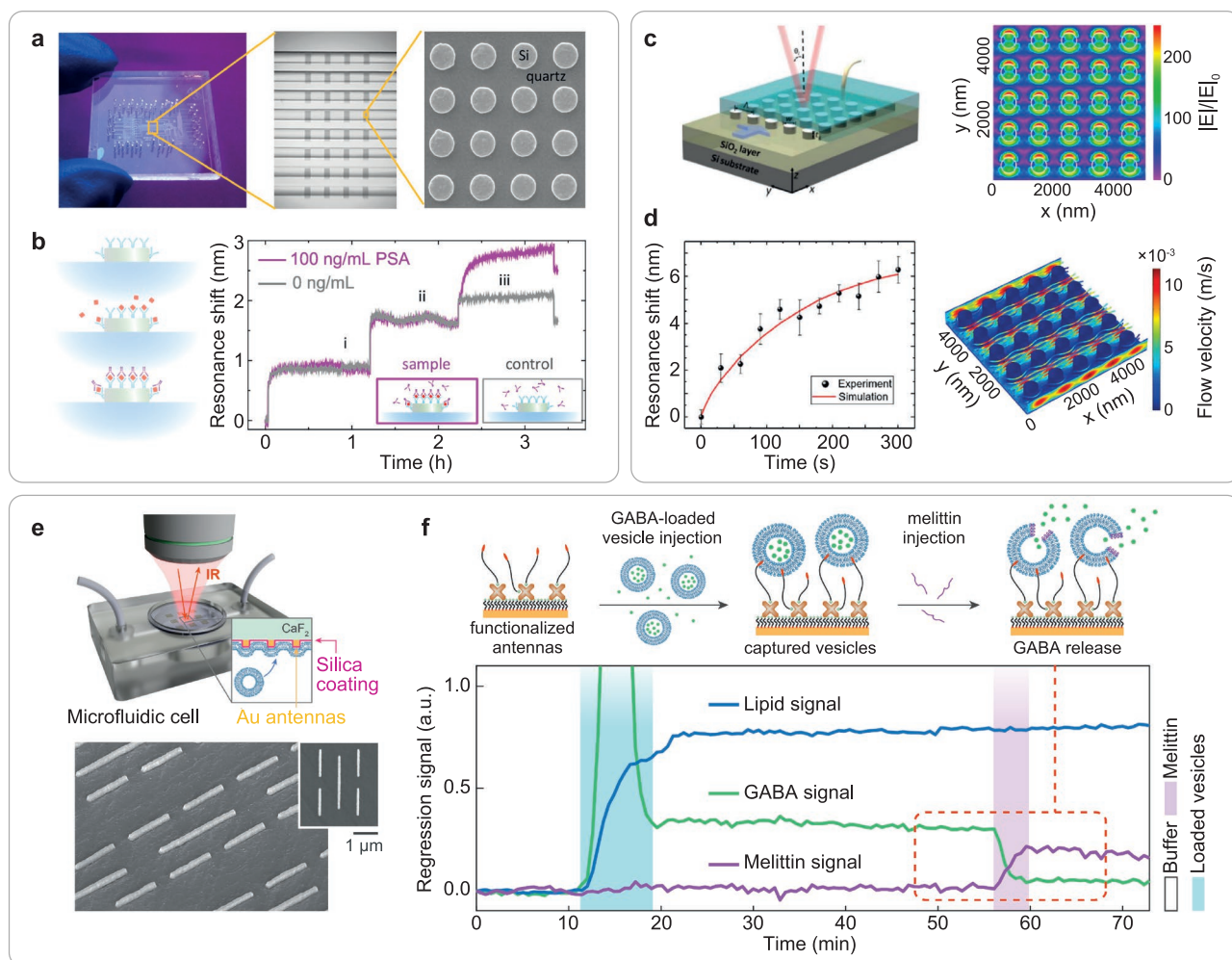


**Figure 5.** Microfluidic channels integrated with nanophotonic sensors. a) Independently controlled microchannels for multiplexed assays with high throughput. b) Sensing of Prostate Specific Antigen (PSA) cancer biomarker with a detection limit down to  $1.6 \text{ ng mL}^{-1}$ . Reproduced with permission.<sup>[21]</sup> Copyright 2017, American Chemical Society. c) Lateral-flow-through biosensor consisting of a periodic array of silicon nanodisks and producing strong near-fields driven by photonic BICs. d) Bonding of a PDMS slab directly on top of the metasurface restricts the flow to the space between the nanodisks, enabling ultrasensitive monitoring of breast cancer biomarkers. Reproduced with permission.<sup>[5]</sup> Copyright 2018, Elsevier B.V. e) SEIRAS-based optofluidic sensor for real-time monitoring of dynamics in complex biological systems using a self-similar multi-resonant metasurface. f) Detection of melittin-induced membrane disruption and release of the neurotransmitter gamma-Aminobutyric acid (GABA) from loaded vesicles. Reproduced with permission.<sup>[95]</sup> Copyright 2018, Springer Nature.

the nanodisks. At the same time, the periodic array of silicon nanodisks supports a high  $Q$  resonance mode with enhanced near-fields exactly overlapping with the region of analyte flow (Figure 5d, right). Such a lateral-flow optofluidic sensor has been shown to detect epidermal growth factor receptor 2 (ErbB2), a protein biomarker for early-stage breast cancer screening, via monitoring resonance wavelength shifts upon specific analyte-ligand binding events at the sensor surface, reaching a limit of detection down to  $0.7 \text{ ng mL}^{-1}$ . They also demonstrated real-time detection with this sensor (Figure 5d, left), showing that the kinetic binding results of ErbB2 and anti-ErbB2 antibody from simulation agreed well with the experimental results.

Additionally, SEIRA-based plasmonic sensors for the real-time detection of chemically specific surface binding events have been demonstrated in aqueous environment by integrating

microfluidic chambers,<sup>[7,95]</sup> enabling diverse biological applications including the monitoring of liquid membranes.<sup>[7]</sup> John-Herpin et al. have demonstrated the real-time probing of protein absorbance signals in aqueous solution with concentrations as low as  $100 \text{ pg mL}^{-1}$  as well as secondary structure differentiation at concentrations on the order of  $500 \text{ ng mL}^{-1}$  using optimized grating order-coupled nanogap antennas.<sup>[38]</sup> Similarly, Rodrigo et al. have demonstrated the real-time monitoring of lipid-protein systems in aqueous environment,<sup>[95]</sup> covering processes such as lipid-protein association, protein-induced disruption of membranes, and vesicular cargo release, by using a multi-resonant mid-IR metasurface (Figure 5e, bottom).<sup>[213]</sup> Significantly, the authors were able to precisely monitor the release dynamics of the neurotransmitter gamma-aminobutyric acid (GABA) from loaded vesicles (Figure 5f). These results suggest that SEIRAS-based optofluidic sensors can open up exciting

applications in the fields of medical diagnostics and pharmacology such as protein misfolding for neurodegenerative disorders, exosomes in cancer, as well as drug release mechanisms from liposomes.

The resonant coupling between the nanoantennas/metasurfaces and the molecular vibration bands can be precisely controlled via the geometry and size of the nanophotonic building blocks, the periodicity, and the surrounding dielectric environment.<sup>[165]</sup> In addition, integration of nanofluidic channels onto the nanophotonic platform is crucial to maximize the utilization of the nanoscale near-fields. However, the external fabrication of nanofluidic channels and the manipulation of fluids within the nanochannels introduces additional complexity because of the associated bonding and alignment processes. Therefore, many recent optofluidic systems have worked toward realizing nanochannels provided by the nanophotonic structure itself, demonstrating hybrid devices with synergistic performance. As mentioned previously, EOT-based resonances sustained in periodic nanohole arrays have first been developed in a flow-over format<sup>[214]</sup> and have later been extended to a flow-through configuration capable of directly driving the fluids to the parallelized nanohole arrays (nanochannels) with rapid diffusion.<sup>[215,216]</sup>

Harnessing a different mechanism for improving diffusion, Barik et al. designed a dielectrophoresis (DEP) enhanced plasmonic sensor based on gold nanohole arrays, which enables more than 1000 times faster binding compared to the purely diffusion-limited case, thereby achieving real-time label-free detection of analytes in a 5  $\mu$ L drop with concentration as low as  $1 \times 10^{-12}$  M in a few minutes (Figure 6a).<sup>[217]</sup> In addition, this configuration reduces the number of adsorption sites in the non-hotspots region, providing a larger spectral shift and improving the detection down to the attomolar (aM) range. Notably, an electric field applied to the plasmonic nanopore can deliver and translocate charged molecules to and away from the hotspots on submillisecond time scales, overcoming the diffusion-limit toward ultratrace or even single molecule detection. Here, the plasmonic nanopore serves as both a sensor and a nanofluidic channel for the active transport of molecules.<sup>[111]</sup> Another example is demonstrated by Dai et al.,<sup>[218]</sup> who developed 3D metallic nanogaps on the inner surface of cylindrical walls of curved nanofluidic channels, simultaneously achieving hotspot creation and fluidic confinement (Figure 6b, top). This hybrid 3D nanocylinder shows a 22 times higher signal intensity for the SERS-based detection of hemoglobin fingerprints

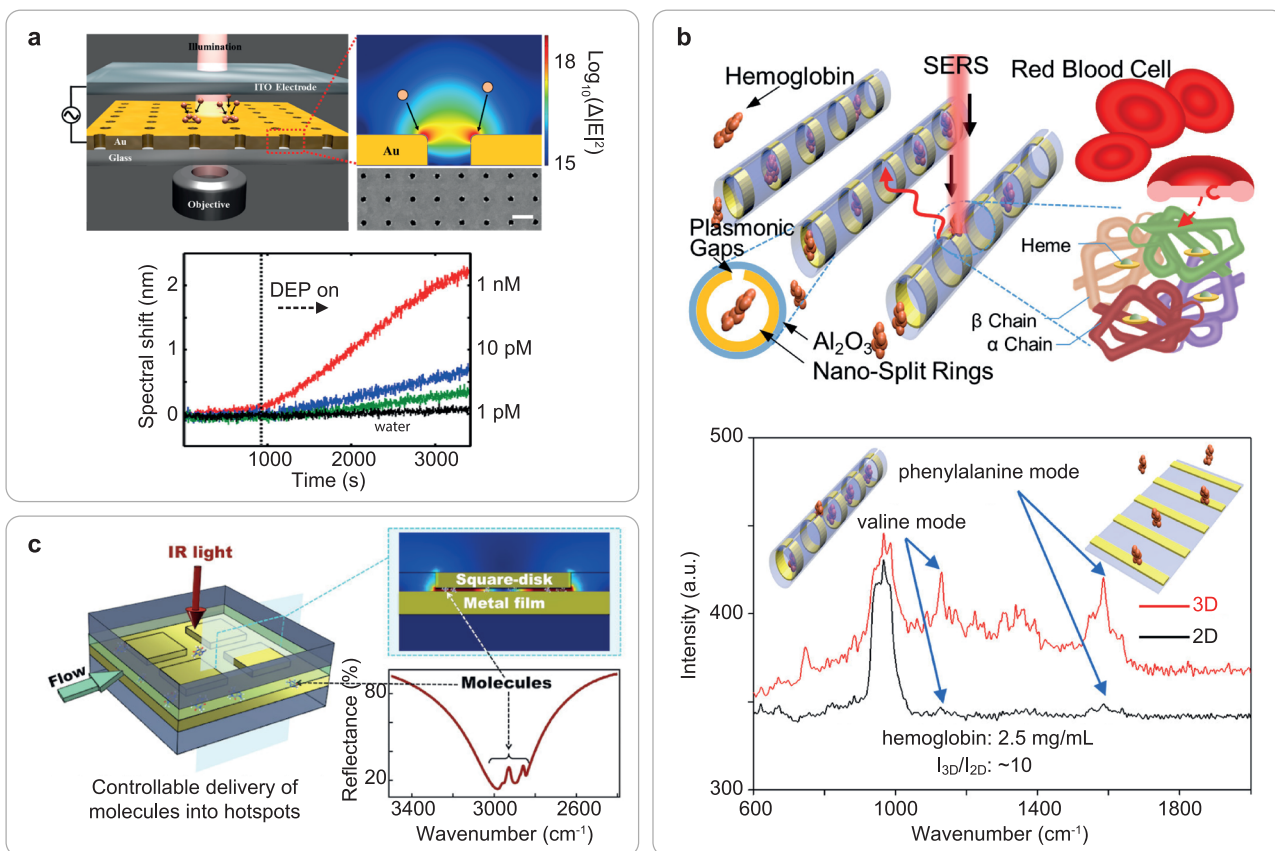


**Figure 6.** Nanofluidic engineering for optimizing spatial overlap between analyte molecules and hotspots of the electromagnetic field. a) DEP-enhanced flow-through periodic nanopore arrays for direct analyte targeting and enhanced sensitivity. Reproduced with permission.<sup>[217]</sup> Copyright 2014, American Chemical Society. b) Nanogaps for simultaneous hotspot generation and analyte confinement based on electron-beam triggered self-assembly. This 3D nanostructure shows 22 times higher hemoglobin sensitivity compared to the corresponding 2D nanostructure. Reproduced with permission.<sup>[218]</sup> Copyright 2020, American Chemical Society. c) Synergistic realization of hotspot generation and analyte confinement in a MIM sensor configuration. Here, the analyte can replace the dielectric spacer layer to fully exploit the nano-spaced hotspots for boosting the sensitivity. Reproduced with permission.<sup>[194]</sup> Copyright 2017, American Chemical Society.

compared to the corresponding 2D nanostructures (Figure 6b, bottom). Such 3D nanogap systems can be realized using electron-beam triggered self-assembly and provide a new approach for exploring 3D nanophotonic structures with combined optofluidic capabilities for highly efficient sensing strategies.

For MIM-based MPAs, hybrid plasmonic-nanofluidic sensors capable of simultaneously confining and coupling the target molecules into the hotspots have also been demonstrated, avoiding the critical issues of severe water absorption typical for SEIRA-based optofluidic sensors.<sup>[194,219]</sup> For example, Le and Tanaka reported a hybrid optofluidic platform for the detection of IR molecular absorption signals, which couples the plasmonic resonators to a metal film through a nanofluidic channel with a depth on the order of tens of nanometers (Figure 6c).<sup>[194]</sup> This hybrid system enables the effective and precise delivery of molecules into the hotspots arising from the interference between the top plasmonic resonators and bottom metal mirror, simultaneously providing quantitative measurements and detection in aqueous solution.

Practical applications in POC diagnostics require the integration of additional functional modules on the optofluidic chip for specimen pre-treatment such as purification, enrichment, and separation. Vázquez-Guardado et al. have demonstrated an optofluidic chip for the detection of dopamine neurotransmitter and nonstructural protein NS1 biomarker directly from blood.<sup>[220,221]</sup> Their optofluidic chip integrates the modules of a plasmonic sensor (Figure 7a) and a plasma separator (Figure 7b),<sup>[221]</sup> achieving NS1 biomarker detection at a concentration of 0.1 to 10  $\mu\text{g mL}^{-1}$  in bovine blood, which covers the clinical threshold of 0.6  $\mu\text{g mL}^{-1}$  linked to a high risk of developing Dengue hemorrhagic fever (Figure 7c).<sup>[222]</sup> Specifically, this plasmonic sensor leverages the hybridization of the LSPR

resonance with an asymmetric Fabry-Perot cavity resonator,<sup>[223]</sup> enabling the early detection of a wide range of viral infections for rapid clinical diagnosis directly from minimally processed biological samples at the POC device level.

Furthermore, Li et al. reported a label-free optofluidic plasmonic biosensor (Figure 7d) for real-time single-cell analysis, where the plasmonic sensor configuration incorporates a specifically designed chamber with low volume and regulation channels made of PDMS for reliable monitoring of cytokine secretion from individual cells over multiple hours (Figure 7e).<sup>[6]</sup> Notably, the optofluidic device was designed to avoid the need to disturb the cell culture and label the secreted cytokine molecules while maintaining the appropriate temperature and humidity conditions required for cell activity and viability. Even though PDMS is a widely used material for cellular bioassays,<sup>[224]</sup> long-term optical monitoring of ultralow volumes in cell culture conditions faces the issue of buffer evaporation due to gas diffusion, thus changing the local refractive index and leading to noticeable optical signal fluctuations that can dominate over the low secretion signals of single cells. To solve this issue, a thin PDMS membrane between the cell culture area and adjacent oxygen equilibrated water channels was implemented to reduce evaporation and maintain the required oxygen level for sustained culturing.<sup>[225]</sup> Functionalization and surface passivation of the sensor module are likewise critical for improving the specific analyte binding efficiency. Normally, the detection of minimally processed raw biological samples is challenging due to non-specific protein adsorption on the sensor surface. To address this, the optical sensor surface was first functionalized by an antifouling SAM, followed by the immobilization of probe molecules for capturing cells (through electrostatic force by positively charged poly-L-lysine polymers)

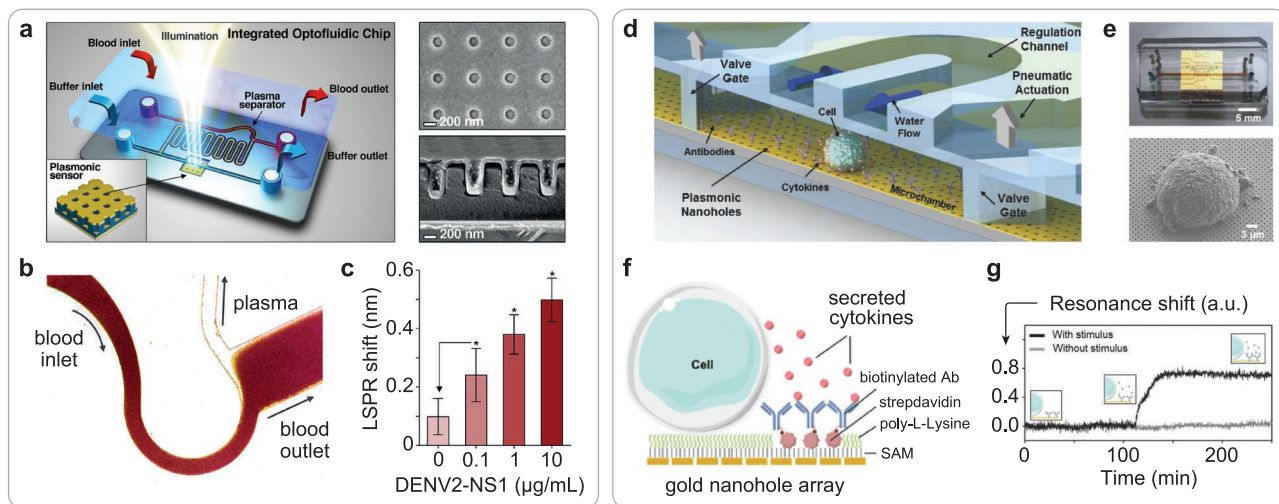


**Figure 7.** Multifunctional optofluidic chips for real-time dynamic studies. a) Integrated optofluidic sensor for NS1 protein detection directly from blood. Schematic of this optofluidic chip incorporating a plasma separator and a plasmonic sensor. SEM images under top- and cross-sectional view show the nanoimprinted optical sensor configuration. b) Microscope photograph of blood plasma separation during NS1 protein detection. c) Resonance shift response as a function of NS1 concentrations in blood together with one control measurement. Reproduced with permission.<sup>[221]</sup> Copyright 2021, American Chemical Society. d) Multifunctional optofluidic system for real-time single cell analysis. Schematic of the system integrating a valve-gated primary microchannel for cell isolation, confinement and analysis, and a regulation channel for controlling cell culture conditions. e) Photograph of the microfluidic device together with a top-view SEM image of a single cell attached on the gold nanohole array chip. f) Schematic of the surface functionalization strategy for cell capture and in-situ detection of secreted cytokines. g) Real-time sensorgram of secreted cytokine detection from a single cell upon chemical stimulus. Reproduced with permission.<sup>[6]</sup> Copyright 2018, Wiley-VCH.

and targets (through streptavidin capture of biotinylated antibodies against the cytokine of interest) (Figure 7f). Upon an external chemical stimulus, there is a distinct resonance shift, indicating that the optofluidic sensor can detect protein secretion from single cells in real time (Figure 7g).

Furthermore, an integrated islet-on-a-chip (IOC) module with a LSPR-based optical sensor has been developed to monitor in-situ insulin secretion from an integrated device, where the insulin is released by pancreatic islets.<sup>[96]</sup> This integrated platform demonstrates the great potential of performing organ-on-a-chip studies with real-time, in-situ and label-free monitoring of different secretion dynamics of cells, tissues and spheroids, providing a robust tool for drug screening, toxicity studies and investigations of metabolic diseases. To close this section and to provide a broader perspective, **Table 1** highlights and compares selected recent examples of

nanophotonics-enabled optofluidic biosensors based on different categories including fluidic channel height/function, target analyte, and detection limit.

## 6. Summary and Outlook

In this review, we have discussed optofluidic biosensors by focusing on the aspects of nanophotonics, micro/nanofluidics, and their synergistic integration. Starting from the physical fundamentals of structured nanophotonic materials, we have introduced SPR and LSPR excitations found in plasmonic materials as well as Mie-type modes and photonic BIC resonances sustained in high refractive index dielectric nanostructures. For all these material platforms, the magnitude of electromagnetic near-field enhancement, the resonance frequency, and the

**Table 1.** Nanophotonics-enabled optofluidic biosensors.

Sensing principle	Nanophotonic configuration	Fluidic channel height	Fluidic channel function	Analytes	Detection limit	Ref.
Refractometry	Au nanohole array	1 mm	analyte transport	IgG2	500 ng mL <sup>-1</sup>	[226]
	Au nanorods	80 μm	acceleration of analyte binding	cytokine biomarker	IL-1β: 1 pg mL <sup>-1</sup> (58 × 10 <sup>-15</sup> M)	[14]
	Au nanohole array	μm scale	analyte transport	virus	< 108 PFU mL <sup>-1</sup>	[227]
	SPR-based chip	50 μm	acceleration of mass transport	bacteria	<i>Escherichia coli</i> : ≈300 CFU mL <sup>-1</sup>	[15]
	Au nanohole array	100 nm	acceleration of mass transport	BSA	1 × 10 <sup>-12</sup> M	[217]
	Au nanohole array	50 μm	analyte transport and plasma separation	dengue virus	NS1 biomarker: 0.1 μg mL <sup>-1</sup>	[221]
	Au nanohole array	μm scale	analyte amplification	exosomes	≈200	[228]
	Au nanohole array	180 μm	cell culturing and analyte transport	cytokine secretion	IL-2 protein: 39 pg mL <sup>-1</sup> (2.6 × 10 <sup>-12</sup> M)	[6]
	silicon metasurface	25 μm	analyte transport	extracellular vesicles	133 × 10 <sup>-15</sup> M	[55]
	dielectric nanohole array	30 μm	analyte transport	IgG2	1 pg mL <sup>-1</sup>	[229]
silicon disk array	μm scale	analyte transport	prostate specific antigen (PSA)	0.69 ng mL <sup>-1</sup>	[21]	
SEF	plasmon-photon hybrid metasurface	30 μm	analyte transport	IgG, cancer marker	IgG: 5 pg mL <sup>-1</sup> (34 × 10 <sup>-15</sup> M), p53 antibody: 50 pg mL <sup>-1</sup>	[230]
	silicon metasurface	μm scale	analyte transport	SARS-Cov-2 RNA	100 mol mL <sup>-1</sup>	[231]
	silicon metasurface	30 μm	analyte transport	antibody/antigen	IgG: 5 pg mL <sup>-1</sup> (34 × 10 <sup>-15</sup> M) CEA: 0.85 pg mL <sup>-1</sup>	[142]
SERS	3D nanosplit rings	1–50 nm	analyte confinement	hemoglobin	2.5 mg mL <sup>-1</sup>	[218]
	Au nanopillars	10 μm	analyte transport and sample separation	N-acetylaspartate	≈pM	[232]
	3D nanogap pillars	30 μm	analyte transport	anticancer drugs	doxorubicin: 10 <sup>-4</sup> M	[233]
	plasmonic nanoslits	sub-10 nm wide	DNA trapping	nucleobase	single-molecule	[234]
	silver colloids	μm scale	analyte transport and pre-sampling	bacteria	100 CFU mL <sup>-1</sup>	[235]
SEIRAS	Al MIM structure	μm scale	analyte trapping	L-proline, D-glucose	1 pg mL <sup>-1</sup>	[236]
	plasmonic structure	500 nm	analyte transport	COVID-19 and mutant virus screening	/	[237]
	grating-order coupled nanogap antennas	μm scale	analyte transport	proteins	100 pg mL <sup>-1</sup>	[38]
	Au nanorods	μm scale	analyte transport	dynamic lipid membrane processes	/	[95]
	Au metasurface	μm scale	analyte transport	single-cell studies	/	[145]

Q factor can be tuned by designing the geometry, orientation, and periodicity of the constituent building blocks. However, due to the intrinsic absorption losses associated with metals, plasmonic resonators can produce heat in the system, potentially damaging the surrounding analyte molecules. Therefore, we highlighted the respective strengths and weaknesses of both metallic and dielectric nanostructures in terms of biosensing applications.

Nanophotonic sensor modules can provide amplified near-fields in nanoscale volumes surrounding the sensor surface, which are highly sensitive to changes of the local environment upon molecular binding and adsorption. The analyte-induced signal can be amplified and transduced by different detection schemes, including refractometry (changes in resonance wavelength, amplitude, and phase induced by refractive index variations), enhanced fluorescence spectroscopy, and vibrational spectroscopy (SERS and SEIRAS). The full utilization of the nanophotonic hotspots requires careful tailoring of analyte flow, which makes the use of micro/nanofluidic approaches critical. Therefore, we have emphasized key aspects of fluidic engineering, including i) multiplexed high throughput assays, ii) analyte delivery to the hotspots, iii) acceleration of analyte-specific binding for lower detection limits toward single molecule detection and fast response times, and iv) pre-processing and integration of other functional modules (e.g., organ-on-chip) for highly automated and in-situ assays. Optofluidic platforms have already demonstrated their great potential for POC devices in resource-limited settings and have enabled real-time, label-free, and in-situ monitoring of dynamics at molecular resolution for clinical diagnostics, drug screening, toxicity studies, and metabolic pathologies with high accuracy and sensitivity. Nevertheless, there are still some fundamental questions and challenges for high-end optofluidic applications in terms of reliable bedside diagnostics, translational medicine, and metabolic diseases, which can motivate and shape upcoming research directions in this exciting field:

**Sensitivity.** Even though high sensitivities within or below clinical detection thresholds have been demonstrated, colorimetric sensing (i.e., the readout of refractometric signal changes by the naked eye) remains elusive. Therefore, further advances in sensitivity are needed, especially for POC devices, either by tailoring the optical sensor units themselves, or by leveraging sophisticated signal processing techniques like artificial intelligence (AI). Similarly, studies of cellular dynamics require improved sensitivities due to the extremely low concentrations of the involved biomolecules and the complex micro-environment. Finally, chiral sensing is crucial for studying the functions of many biosystems, but likewise requires very high sensitivities to enable effective enantiomeric differentiation.

**Specificity.** Many widely implemented optical biosensors operate in a homogeneous environment (i.e., in water or buffer solution), which greatly simplifies the optical sensing process. However, sensing in complex heterogeneous media poses significant challenges because of high background signals associated with the biological matrix, e.g., when targeting the direct detection of biomarkers from bodily fluids without sample pre-processing. To address this challenge, surface functionalization of the optical sensors needs to be implemented through surface chemistry and the selection of appropriate optical sensor

materials. Alternatively, functional modules can be implemented on the optofluidic chip to achieve purification and separation for the subsequent sensing steps. Therefore, it is crucial to focus on the optofluidic integration of such functional modules to bring this technology to practical POC applications.

**On-chip integration.** Going beyond the integration of nanophotonic sensors and fluidic compartments, it is highly desirable to integrate the remaining sensor components such as light sources, spectrometers, and fluidic drivers onto the chip as well. Full monolithic integration of all sensor components greatly increases the portability and robustness of the sensor, which is especially significant for field-deployed applications in resource-limited geographic regions. In this context, important trade-offs between sensitivity/detection limit (research use) and portability (POC use) will have to be considered.

**Scalability.** Versatile fabrication methods such as electron beam lithography, focused ion beam lithography, and nano-stencil lithography are available and widely used for optofluidic device implementations. However, real-world applications, specifically in diagnostics, will require high yield, as well as cost- and time-efficient fabrication methods to scale up these technologies for use in laboratories, hospitals, and patients' homes everywhere.

## Acknowledgements

This article is part of the *Advanced Optical Materials* Hall of Fame article series, which recognizes the excellent contributions of leading researchers to the field of optical materials science. This work was funded by the Deutsche Forschungsgemeinschaft (DFG, German Research Foundation) under grant numbers EXC 2089/1 – 390776260 (Germany's Excellence Strategy) and TI 1063/1 (Emmy Noether Program), the Bavarian program Solar Energies Go Hybrid (SolTech) and the Center for NanoScience (CeNS). S.A.M. additionally acknowledges the Lee-Lucas Chair in Physics.

Open access funding enabled and organized by Projekt DEAL.

## Conflict of Interest

The authors declare no conflict of interest.

## Keywords

diagnostics, nanophotonics, optofluidic sensing, refractometry, surface-enhanced spectroscopy

Received: November 2, 2021

Revised: December 15, 2021

Published online: February 22, 2022

- [1] H. Xin, B. Namgung, L. P. Lee, *Nat. Rev. Mater.* **2018**, *3*, 228.
- [2] P. Ray, A. J. Steckl, *ACS Sens.* **2019**, *4*, 1346.
- [3] J. Tu, R. M. Torrente-rodríguez, M. Wang, W. Gao, *Adv. Funct. Mater.* **2020**, *30*, 1906713.
- [4] R. Semenyshyn, M. Hentschel, C. Stanglmair, T. Teutsch, C. Tarin, C. Pacholski, H. Giessen, F. Neubrech, *Nano Lett.* **2019**, *19*, 1.
- [5] Y. Wang, A. Ali, E. K. C. Chow, L. Dong, M. Lu, *Biosens. Bioelectron.* **2018**, *107*, 224.



- [6] X. Li, M. Soler, C. Szydzik, J. Khoshmanesh, Khashayar, Schmidt, G. Coukos, A. Mitchell, H. Altug, *Small* **2018**, *14*, 1800698.
- [7] O. Limaj, D. Etezadi, N. J. Wittenberg, D. Rodrigo, D. Yoo, S. Oh, H. Altug, *Nano Lett.* **2016**, *16*, 1502.
- [8] J. Wang, M. M. Sanchez, Y. Yin, R. Herzer, L. Ma, O. G. Schmidt, *Adv. Mater. Technol.* **2020**, *5*, 1901138.
- [9] H. Marks, M. Schechinger, J. Garza, A. Locke, G. Coté, *Nanophotonics* **2017**, *6*, 681.
- [10] Y. S. Zhang, J. Alemana, S. R. Shin, T. Kilica, D. Kim, S. A. M. Shaegh, S. Massa, R. Riahi, S. Chae, N. Hua, H. Avci, W. Zhang, A. Silvestri, A. S. Nezhad, A. Manbohi, F. De Ferrari, A. Polini, G. Calzone, N. Shaikh, P. Alerasool, E. Budina, J. Kang, N. Bhise, J. Ribas, A. Pourmand, A. Skardal, T. Shupe, C. E. Bishop, M. R. Dokmeci, A. Atala, et al., *Proc. Natl. Acad. Sci. USA* **2017**, *12*, E2293.
- [11] R. O. Rodrigues, P. C. Sousa, J. Gaspar, M. Bañobre-lópez, R. Lima, G. Minas, *Small* **2020**, *16*, 2003517.
- [12] S. Kumar, S. Cherukulappurath, T. W. Johnson, S. Oh, *Chem. Mater.* **2014**, *26*, 6523.
- [13] M. P. Jonsson, A. B. Dahlin, L. Feuz, S. Petronis, F. Ho, *Anal. Chem.* **2010**, *82*, 2087.
- [14] U. Cytokine, Y. Song, P. Chen, M. T. Chung, R. Nidetz, Y. Park, Z. Liu, W. Mchugh, T. T. Cornell, J. Fu, K. Kurabayashi, *Nano Lett.* **2017**, *17*, 2374.
- [15] D. D. Galvan, V. Parekh, E. Liu, E. Liu, Q. Yu, *Anal. Chem.* **2018**, *90*, 14635.
- [16] A. V Vlassov, S. Magdaleno, R. Setterquist, R. Conrad, *Biochim. Biophys. Acta* **2012**, *1820*, 940.
- [17] Z. Altintas, M. Akgun, G. Kokturk, Y. Uludag, *Biosens. Bioelectron.* **2018**, *100*, 541.
- [18] G. C. M. de Oliveira, J. H. de S. Carvalho, L. C. Brazaca, N. C. S. Vieira, B. C. Janegitz, *Biosens. Bioelectron.* **2020**, *152*, 112016.
- [19] S. Jones, D. Andre, P. Karpinski, M. Käll, *ACS Photonics* **2018**, *5*, 2878.
- [20] S. S. Acimovic, M. A. Ortega, V. Sanz, J. Berthelot, J. L. Garcia-cordero, J. Renger, S. J. Maerkl, M. P. Kreuzer, R. Quidant, *Nano Lett.* **2014**, *14*, 2636.
- [21] O. Yavas, M. Svedendahl, P. Dobosz, V. Sanz, R. Quidant, *Nano Lett.* **2017**, *17*, 4421.
- [22] S. A. Maier, *Plasmonics Fundamentals and Applications*, Springer, New York **2007**.
- [23] J. R. Sambles, G. W. Bradbery, F. Yang, *Contemp. Phys.* **1991**, *32*, 173.
- [24] E. Kretschmann, H. Raether, *Z. Naturforsch. A* **1968**, *23*, 2135.
- [25] A. S. Lambert, S. N. Valiulis, A. S. Malinick, I. Tanabe, Q. Cheng, *Anal. Chem.* **2020**, *92*, 8654.
- [26] B. Hecht, H. Bielefeldt, L. Novotny, Y. Inouye, D. W. Pohl, *Phys. Rev. Lett.* **1996**, *77*, 1889.
- [27] R. H. Ritchie, E. T. Arakawa, J. J. Cowan, R. N. Hamm, *Phys. Rev. Lett.* **1968**, *21*, 1530.
- [28] D. Cai, Y. Lu, K. Lin, P. Wang, H. Ming, *Opt. Express* **2008**, *16*, 14597.
- [29] K. L. Kelly, E. Coronado, L. L. Zhao, G. C. Schatz, *J. Phys. Chem. B* **2003**, *107*, 668.
- [30] L. Le Thi Ngoc, M. Jin, J. Wiedemair, A. van den Berg, E. T. Carlen, *ACS Nano* **2013**, *7*, 5223.
- [31] J. Nam, J. Oh, H. Lee, Y. D. Suh, *Acc. Chem. Res.* **2016**, *49*, 2746.
- [32] J. Wang, M. Jin, Y. Gong, H. Li, S. Wu, Z. Zhang, G. Zhou, L. Shui, *Lab Chip* **2017**, *17*, 1970.
- [33] L. Dong, X. Yang, C. Zhang, B. Cerjan, L. Zhou, M. L. Tseng, Y. Zhang, A. Alabastri, P. Nordlander, N. J. Halas, *Nano Lett.* **2017**, *17*, 5768.
- [34] T. G. Mayerhöfer, J. Popp, *Nanophotonics* **2018**, *7*, 39.
- [35] S. Bagheri, K. Weber, T. Gissibl, T. Weiss, F. Neubrech, H. Giessen, *ACS Photonics* **2015**, *2*, 779.
- [36] J. Olson, A. Manjavacas, L. Liu, W. Chang, B. Foerster, N. S. King, *Proc. Natl. Acad. Sci. USA* **2014**, *111*, 14348.
- [37] K. Su, Q. Wei, X. Zhang, *Nano Lett.* **2003**, *3*, 1087.
- [38] A. John-herpin, A. Tittl, H. Altug, *ACS Photonics* **2018**, *5*, 4117.
- [39] B. Auguie, W. L. Barnes, *Phys. Rev. Lett.* **2008**, *143902*, 1.
- [40] H. Raether, *Surface Plasmons on Smooth and Rough Surfaces and on Gratings*, Springer, New York **1988**.
- [41] M. Svedendahl, S. Chen, A. Dmitriev, M. Kall, *Nano Lett.* **2009**, *9*, 4428.
- [42] M. Piliarik, J. Homola, *Opt. Express* **2009**, *17*, 16505.
- [43] C. Rosman, J. Prasad, A. Neiser, A. Henkel, J. Edgar, C. Sönnichsen, *Nano Lett.* **2013**, *13*, 3243.
- [44] K. M. Mayer, J. H. Hafner, *Chem. Rev.* **2011**, *111*, 3828.
- [45] B. Luk'yanchuk, N. Zheludev, S. A. Maier, N. J. Halas, P. Nordlander, H. Giessen, C. T. Chong, *Nat. Mater.* **2010**, *9*, 707.
- [46] M. F. Limonov, M. V Rybin, A. N. Poddubny, Y. S. Kivshar, *Nat. Photonics* **2017**, *11*, 543.
- [47] C. Yan, K. Yang, O. J. F. Martin, *Light: Sci. Appl.* **2017**, *6*, 17017.
- [48] S. Simoncelli, Y. Li, E. Cortés, S. A. Maier, *Nano Lett.* **2018**, *18*, 3400.
- [49] Y. Francescato, V. Giannini, S. A. Maier, *ACS Nano* **2012**, *6*, 1830.
- [50] B. Hopkins, A. N. Poddubny, A. E. Miroshnichenko, Y. S. Kivshar, *Laser Photonics Rev.* **2016**, *10*, 137.
- [51] S. Campione, C. Guclu, R. Ragan, F. Capolino, *ACS Photonics* **2014**, *1*, 254.
- [52] Y. K. Srivastava, M. Manjappa, L. Cong, W. Cao, I. Al-Naib, W. Zhang, R. Singh, *Adv. Opt. Mater.* **2016**, *4*, 457.
- [53] C. Wu, A. B. Khanikaev, R. Adato, N. Arju, A. A. Yanik, H. Altug, G. Shvets, *Nat. Mater.* **2011**, *11*, 69.
- [54] I. Barth, S. Johnson, T. F. Krauss, *Light: Sci. Appl.* **2020**, *9*, 96.
- [55] Y. Jahani, E. R. Arvelo, F. Yesilkoy, K. Koshelev, M. De Palma, Y. Kivshar, H. Altug, *Nat. Commun.* **2021**, *12*, 3246.
- [56] J. Bohn, T. Bucher, K. E. Chong, A. Komar, D. Choi, D. N. Neshev, Y. S. Kivshar, T. Pertsch, I. Staude, *Nano Lett.* **2018**, *18*, 3461.
- [57] Y. Kivshar, A. Miroshnichenko, *Opt. Photonics News* **2017**, *28*, 24.
- [58] S. R. Amanaganti, M. Ravnik, J. Dontabhaktuni, *Sci. Rep.* **2020**, *10*, 15599.
- [59] I. Staude, J. Schilling, *Nat. Photonics* **2017**, *11*, 274.
- [60] P. D. Terekhov, K. V. Baryshnikova, A. S. Shalin, A. Karabchevsky, A. B. Evlyukhin, *Opt. Lett.* **2017**, *42*, 835.
- [61] A. B. Evlyukhin, S. M. Novikov, U. Zywietz, R. L. Eriksen, C. Reinhardt, S. I. Bozhevolnyi, B. N. Chichkov, *Nano Lett.* **2012**, *12*, 3749.
- [62] F. Yesilkoy, E. R. Arvelo, Y. Jahani, M. Liu, A. Tittl, V. Cevher, Y. Kivshar, H. Altug, *Nat. Photonics* **2019**, *13*, 390.
- [63] S. Romano, M. Mangini, E. Penzo, S. Cabrini, A. C. De Luca, I. Rendina, V. Mocella, G. Zito, *ACS Nano* **2020**, *14*, 15417.
- [64] M. L. Tseng, Y. Jahani, A. Leitis, H. Altug, *ACS Photonics* **2021**, *8*, 47.
- [65] M. L. Solomon, J. Hu, M. Lawrence, A. Garc, J. A. Dionne, *ACS Photonics* **2019**, *6*, 43.
- [66] J. A. Fan, K. Bao, C. Wu, J. Bao, R. Bardhan, N. J. Halas, V. N. Manoharan, G. Shvets, P. Nordlander, F. Capasso, *Nano Lett.* **2010**, *10*, 4680.
- [67] C. F. Bohren, *Absorption and Scattering of Light by Small Particles*, John Wiley & Sons, New York **2008**.
- [68] S. Kruk, Y. Kivshar, *ACS Photonics* **2017**, *4*, 2638.
- [69] J. Jang, T. Badloe, Y. Yang, T. Lee, J. Mun, J. Rho, *ACS Nano* **2020**, *14*, 15317.
- [70] J. Jeong, M. D. Gold, S. Campione, J. L. Briscoe, P. P. Vabishchevich, J. Nogan, M. B. Sinclair, T. S. Luk, I. Brener, *ACS Photonics* **2020**, *7*, 1699.
- [71] A. E. Krasnok, A. E. Miroshnichenko, P. A. Belov, Y. S. Kivshar, *Opt. Express* **2012**, *20*, 20599.

- [72] Z. Sadrieva, K. Frizyuk, M. Petrov, Y. Kivshar, A. Bogdanov, *Phys. Rev. B* **2019**, *100*, 115303.
- [73] K. Koshelev, Y. Kivshar, *ACS Photonics* **2021**, *8*, 102.
- [74] N. O. Länk, M. Käll, T. J. Antosiewicz, *ACS Photonics* **2019**, *6*, 1706.
- [75] R. M. Bakker, D. Permyakov, Y. F. Yu, D. Markovich, R. P.-D. L. Gonzaga, A. Samusev, Y. Kivshar, B. Luk'yanchuk, A. I. Kuznetsov, *Nano Lett.* **2015**, *15*, 2137.
- [76] M. K. Schmidt, R. Esteban, J. J. S'aenz, I. Su'arez-Lacalle, S. Mackowski, J. Aizpurua, *Opt. Express* **2012**, *20*, 13636.
- [77] P. Albella, M. A. Poyli, M. K. Schmidt, S. A. Maier, F. Moreno, J. Jose, J. Aizpurua, *J. Phys. Chem. B* **2013**, *117*, 13573.
- [78] M. Caldarola, P. Albella, E. Cortes, M. Rahmani, T. Roschuk, G. Grinblat, R. F. Oulton, A. V. Bragas, S. A. Maier, *Nat. Commun.* **2015**, *6*, 1.
- [79] K. Koshelev, S. Kruk, E. Melik-gaykazyan, J. Choi, A. Bogdanov, H. Park, Y. Kivshar, *Science* **2020**, *367*, 288.
- [80] K. Koshelev, S. Lepeshov, M. Liu, A. Bogdanov, Y. Kivshar, *Phys. Rev. Lett.* **2018**, *121*, 193903.
- [81] H. Friedrich, D. Wintgen, *Phys. Rev. A* **1985**, *32*, 3231.
- [82] C. W. Hsu, B. Zhen, A. D. Stone, J. D. Joannopoulos, M. Soljac, *Nat. Rev. Mater.* **2016**, *1*, 16048.
- [83] M. Rybin, Y. Kivshar, *Nature* **2017**, *541*, 164.
- [84] E. Melik-gaykazyan, K. Koshelev, J. Choi, S. S. Kruk, A. Bogdanov, H. Park, Y. Kivshar, *Nano Lett.* **2021**, *21*, 1765.
- [85] M. Odit, K. Koshelev, S. Gladyshev, K. Ladutenko, Y. Kivshar, A. Bogdanov, *Adv. Mater.* **2021**, *33*, 2003804.
- [86] C. W. Hsu, B. Zhen, J. Lee, S. Chua, S. G. Johnson, J. D. Joannopoulos, M. Soljac, *Nature* **2013**, *499*, 188.
- [87] Y. Chen, C. Zhao, Y. Zhang, C. Qiu, *Nano Lett.* **2020**, *20*, 8696.
- [88] J. Wang, J. Kühne, T. Karamanos, C. Rockstuhl, S. A. Maier, A. Tittl, *Adv. Funct. Mater.* **2021**, *31*, 2104652.
- [89] A. G. Brolo, *Nat. Photonics* **2012**, *6*, 709.
- [90] A. I. Kuznetsov, A. E. Miroshnichenko, Y. H. Fu, J. Zhang, B. Luk, *Sci. Rep.* **2012**, *2*, 492.
- [91] O. Yavas, M. Svedendahl, R. Quidant, *ACS Nano* **2019**, *13*, 4582.
- [92] A. Belushkin, F. Yesilkoy, H. Altug, *ACS Nano* **2018**, *12*, 4453.
- [93] A. Xomalis, X. Zheng, A. Demetriadou, A. Mart, R. Chikkaraddy, J. J. Baumberg, *Nano Lett.* **2021**, *21*, 2512.
- [94] A. John-herpin, D. Kavungal, L. Von Mücke, H. Altug, *Adv. Mater.* **2021**, *33*, 2006054.
- [95] D. Rodrigo, A. Tittl, N. Ait-Bouziad, A. John-Herpin, O. Limaj, C. Kelly, D. Yoo, N. J. Wittenberg, S. H. Oh, H. A. Lashuel, H. Altug, *Nat. Commun.* **2018**, *9*, 2160.
- [96] M. A. Ortega, J. Rodríguez-Comas, O. Yavas, F. Velasco-Mallorquí, J. Balaguer-Trias, V. Parra, A. Novials, J. M. Servitja, R. Quidant, J. Ramón-Azcón, *Biosensors* **2021**, *11*, 138.
- [97] A. Belushkin, F. Yesilkoy, J. J. González-lópez, J. C. Ruiz-rodríguez, R. Ferrer, A. Fàbrega, H. Altug, *Small* **2019**, *16*, 1906108.
- [98] J. Masson, *Analyst* **2020**, *145*, 3776.
- [99] H. Im, N. J. Wittenberg, A. Lesuffleur, N. C. Lindquist, S.-H. Oh, *Chem. Sci.* **2010**, *1*, 688.
- [100] H. Im, H. Shao, Y. Il Park, V. M. Peterson, C. M. Castro, R. Weissleder, H. Lee, *Nat. Biotechnol.* **2014**, *32*, 490.
- [101] S. Chen, M. Svedendahl, R. P. Van Duyne, K. Mikael, *Nano Lett.* **2011**, *11*, 1826.
- [102] L. J. Sherry, R. Jin, C. A. Mirkin, G. C. Schatz, R. P. Van Duyne, *Nano Lett.* **2006**, *6*, 2060.
- [103] M. Mivelle, T. S. van Zanten, L. Neumann, N. F. van Hulst, M. F. Garcia-Parajo, *Nano Lett.* **2012**, *12*, 5972.
- [104] M. L. Juan, M. Righini, R. Quidant, *Nat. Photonics* **2011**, *5*, 349.
- [105] A. E. Cetin, A. F. Coskun, B. C. Galarreta, M. Huang, D. Herman, A. Ozcan, H. Altug, *Light: Sci. Appl.* **2014**, *3*, e122.
- [106] T. W. Ebbesen, H. J. Lezec, H. F. Ghaemi, T. Thio, P. A. Wolff, *Nature* **1998**, *391*, 667.
- [107] F. Anggoro, A. Nugroho, D. Albinsson, T. J. Antosiewicz, C. Langhammer, *ACS Nano* **2020**, *14*, 2345.
- [108] H. Im, A. Lesuffleur, N. C. Lindquist, S. Oh, *Anal. Chem.* **2009**, *81*, 2854.
- [109] K. V. Sreekanth, S. Sreejith, S. Han, X. Chen, H. Sun, C. T. Lim, R. Singh, *Nat. Commun.* **2018**, *9*, 369.
- [110] A. B. Taylor, P. Zijlstra, *ACS Sens.* **2017**, *2*, 1103.
- [111] X. Shi, D. V. Verschuere, C. Dekker, *Nano Lett.* **2018**, *18*, 8003.
- [112] I. Ament, J. Prasad, A. Henkel, S. Schmachtel, *Nano Lett.* **2012**, *12*, 1092.
- [113] M. A. Beuwer, M. W. J. Prins, P. Zijlstra, *Nano Lett.* **2015**, *15*, 3507.
- [114] Y. Pang, R. Gordon, *Nano Lett.* **2012**, *12*, 402.
- [115] J. Weiner, *Rep. Prog. Phys.* **2009**, *72*, 064401.
- [116] J. Yan, P. Liu, Z. Lin, G. Yang, *Nanoscale* **2016**, *8*, 5996.
- [117] N. Bosio, H. Šípová-jungová, N. O. Länk, T. J. Antosiewicz, R. Verre, M. Käll, *ACS Photonics* **2019**, *6*, 1556.
- [118] I. Teraoka, S. Arnold, *J. Opt. Soc. Am. B* **2006**, *23*, 1381.
- [119] W. Shi, F. Fan, Z. Zhang, T. Zhang, S. Li, X. Wang, *Appl. Sci.* **2021**, *11*, 8892.
- [120] J. Kumar, H. Eraña, E. López-martínez, N. Claes, V. F. Martín, D. M. Solís, S. Bals, A. L. Cortajarena, J. Castillab, L. M. Liz-Marzán, *Proc. Natl. Acad. Sci. USA* **2020**, *115*, 3225.
- [121] T. Kimura, K. Hamase, Y. Miyoshi, R. Yamamoto, K. Yasuda, M. Mita, H. Rakugi, T. Hayashi, Y. Isaka, *Sci. Rep.* **2016**, *6*, 1.
- [122] L. A. Nguyen, H. He, C. Pham-huy, *Int. J. Biomed. Sci.* **2006**, *2*, 85.
- [123] Y. Tang, A. E. Cohen, *Phys. Rev. Lett.* **2010**, *104*, 163901.
- [124] M. V. Gorkunov, A. A. Antonov, Y. S. Kivshar, *Phys. Rev. Lett.* **2020**, *125*, 93903.
- [125] M. L. Nesterov, X. Yin, M. Scha, H. Giessen, T. Weiss, *ACS Photonics* **2016**, *3*, 578.
- [126] E. Mohammadi, A. Tittl, K. L. Tsakmakidis, T. V. Raziman, A. G. Curto, *ACS Photonics* **2021**, *8*, 1754.
- [127] A. Garcia-Etxarri, J. A. Dionne, *Phys. Rev. B* **2013**, *87*, 235409.
- [128] W. Ma, H. Kuang, L. Xu, L. Ding, C. Xu, L. Wang, N. A. Kotov, *Nat. Commun.* **2013**, *4*, 2689.
- [129] E. Hendry, T. Carpy, J. Johnston, M. Popland, R. V. Mikhaylovskiy, A. J. Laphorn, S. M. Kelly, L. D. Barron, N. Gadegaard, M. Kadodwala, *Nat. Nanotechnol.* **2010**, *5*, 783.
- [130] Y. Zhao, A. N. Askarpour, L. Sun, J. Shi, X. Li, A. Alu, *Nat. Commun.* **2017**, *8*, 14180.
- [131] S. M. Fothergill, C. Joyce, F. Xie, *Nanoscale* **2018**, *10*, 20914.
- [132] K. J. Russell, T. Liu, S. Cui, E. L. Hu, *Nat. Photonics* **2012**, *6*, 459.
- [133] P. K. Jain, M. A. El-sayed, *Chem. Phys. Lett.* **2010**, *487*, 153.
- [134] W. L. Barnes, *J. Mod. Opt.* **1998**, *45*, 661.
- [135] Y. Chen, K. Munechika, D. S. Ginger, *Nano Lett.* **2007**, *7*, 690.
- [136] A. Rose, T. B. Hoang, F. McGuire, J. J. Mock, C. Ciraci, D. R. Smith, M. H. Mikkelsen, *Nano Lett.* **2014**, *14*, 4797.
- [137] G. Lu, T. Zhang, W. Li, L. Hou, J. Liu, Q. Gong, *J. Phys. Chem. C* **2011**, *115*, 15822.
- [138] A. I. Dragan, E. S. Bishop, J. R. Casas-finet, R. J. Strouse, J. McGivney, M. A. Schenerman, C. D. Geddes, *Plasmonics* **2012**, *7*, 739.
- [139] D. F. Cruz, C. M. Fontes, D. Semeniak, J. Huang, A. Hucknall, A. Chilkoti, M. H. Mikkelsen, *Nano Lett.* **2020**, *20*, 4330.
- [140] J. Hwang, S. Park, J. Son, J. W. Park, J. Nam, *Nano Lett.* **2021**, *21*, 2132.
- [141] F. Zang, Z. Su, L. Zhou, K. Konduru, G. Kaplan, S. Y. Chou, *Adv. Mater.* **2019**, *31*, 1902331.
- [142] M. Iwanaga, *ACS Nano* **2020**, *14*, 17458.
- [143] J. Cambiasso, G. Grinblat, Y. Li, A. Rakovich, E. Cortés, S. A. Maier, *Nano Lett.* **2017**, *17*, 1219.
- [144] R. Regmi, J. Berthelot, P. M. Winkler, M. Mivelle, J. Proust, F. Bed, I. Ozerov, T. Begou, J. Lumeau, H. Rigneault, M. F. García-Parajo, S. Bidault, J. Wenger, N. Bonod, *Nano Lett.* **2016**, *16*, 5143.

- [145] S. H. Huang, J. Li, Z. Fan, R. Delgado, G. Shvets, *Lab Chip* **2021**, 21, 3991.
- [146] H. Im, K. C. Bantz, N. C. Lindquist, C. L. Haynes, S. Oh, *Nano Lett.* **2010**, 10, 2231.
- [147] S. Laing, L. E. Jamieson, K. Faulds, D. Graham, *Nat. Rev. Chem.* **2017**, 1, 0060.
- [148] J. Wang, P. W. H. Pinkse, L. I. Segerink, J. C. T. Eijkel, *ACS Nano* **2021**, 15, 9299.
- [149] Z. Dong, V. Deckert, J. Popp, *Chem. Soc. Rev.* **2017**, 46, 3945.
- [150] K. K. Maiti, A. Samant, M. Vendrell, K.-S. Soh, M. Olivoa, Y.-T. Chang, *Chem. Commun.* **2011**, 47, 3514.
- [151] G. Kuku, M. Altunbek, M. Culha, *Anal. Chem.* **2017**, 89, 11160.
- [152] J. Taylor, A. Huefner, L. Li, S. Mahajan, *Analyst* **2016**, 141, 5037.
- [153] W. Nam, X. Ren, S. A. S. Tali, P. Ghassemi, I. Kim, M. Agah, W. Zhou, *Nano Lett.* **2019**, 19, 7273.
- [154] C. Zong, M. Xu, L. Xu, T. Wei, X. Ma, X. Zheng, R. Hu, B. Ren, *Chem. Rev.* **2018**, 118, 4946.
- [155] P. Y. Liu, L. K. Chin, W. Ser, H. F. Chen, C.-M. Hsieh, C.-H. Lee, K.-B. Sung, T. C. Ayi, P. H. Yap, B. Liedberg, K. Wang, T. Bourouina, Y. Leprince-Wang, *Lab Chip* **2016**, 16, 634.
- [156] P. R. Miller, R. M. Taylor, B. Q. Tran, G. Boyd, T. Glaros, V. H. Chavez, R. Krishnakumar, A. Sinha, K. Poorey, K. P. Williams, S. S. Branda, J. T. Baca, R. Polsky, *Commun. Biol.* **2018**, 1, 173.
- [157] Z. Wang, J. Luan, A. Seth, L. Liu, M. You, P. Gupta, P. Rath, Y. Wang, S. Cao, Q. Jiang, X. Zhang, R. Gupta, Q. Zhou, J. J. Morrissey, E. L. Scheller, J. S. Rudra, S. Singamaneni, *Nat. Biomed. Eng.* **2021**, 5, 64.
- [158] J. E. Park, N. Yonet-tanyeri, E. Vander Ende, A. Henry, B. E. P. White, M. Mrksich, R. P. Van Duyn, *Nano Lett.* **2019**, 19, 6862.
- [159] G. Baffou, R. Quidant, *Laser Photonics Rev.* **2013**, 7, 171.
- [160] M. Mahmoudi, S. E. Lohse, C. J. Murphy, A. Fathizadeh, A. Montazeri, K. S. Suslick, *Nano Lett.* **2014**, 14, 6.
- [161] C. F. Kenworthy, L. P. Stoevelaar, A. J. Alexander, G. Gerini, *Sci. Rep.* **2021**, 11, 6873.
- [162] S. Romano, G. Zito, S. Manago, G. Cala, E. Penzo, S. Cabrini, A. C. De Luca, V. Mocella, *J. Phys. Chem. C* **2018**, 122, 19738.
- [163] I. Alessandri, J. R. Lombardi, *Chem. Rev.* **2016**, 116, 14921.
- [164] A. Hartstein, J. R. Kirtley, J. C. Tsang, *Phys. Rev. Lett.* **1980**, 45, 201.
- [165] F. Neubrech, C. Huck, K. Weber, A. Pucci, H. Giessen, *Chem. Rev.* **2017**, 117, 5110.
- [166] C. Huck, J. Vogt, M. Sendner, D. Hengstler, F. Neubrech, A. Pucci, *ACS Photonics* **2015**, 2, 1489.
- [167] X. Chen, C. Cirac, D. R. Smith, S. Oh, *Nano Lett.* **2015**, 15, 107.
- [168] E. Cubukcu, S. Zhang, Y.-S. Park, G. Bartal, X. Zhang, *Appl. Phys. Lett.* **2009**, 95, 043113.
- [169] L. V. Brown, X. Yang, K. Zhao, B. Y. Zheng, P. Nordlander, N. J. Halas, *Nano Lett.* **2015**, 15, 1272.
- [170] A. E. Cetin, D. Etezadi, H. Altug, *Adv. Opt. Mater.* **2014**, 2, 866.
- [171] C. Huck, A. Toma, F. Neubrech, M. Chirumamilla, J. Vogt, F. De Angelis, A. Pucci, *ACS Photonics* **2015**, 2, 497.
- [172] C. M. Watts, X. Liu, W. J. Padilla, *Adv. Opt. Mater.* **2012**, 24, OP98.
- [173] K. Chen, R. Adato, H. Altug, *ACS Nano* **2012**, 6, 7998.
- [174] D. Ji, A. Cheney, N. Zhang, H. Song, J. Gao, X. Zeng, H. Hu, S. Jiang, Z. Yu, Q. Gan, *Adv. Opt. Mater.* **2017**, 5, 1700223.
- [175] D. Yoo, D. A. Mohr, F. Vidal-codina, A. John-herpin, M. Jo, S. Kim, J. Matson, J. D. Caldwell, H. Jeon, N. Nguyen, L. Martin-moreno, J. Peraire, H. Altug, S. Oh, *Nano Lett.* **2018**, 18, 1930.
- [176] A. A. E. Saleh, J. A. Dionne, *Nano Lett.* **2012**, 12, 5581.
- [177] X. Hui, C. Yang, D. Li, X. He, H. Huang, H. Zhou, M. Chen, C. Lee, X. Mu, *Adv. Sci.* **2021**, 8, 2100583.
- [178] X. Liu, T. Starr, A. F. Starr, W. J. Padilla, *Phys. Rev. Lett.* **2010**, 104, 207403.
- [179] A. Tittl, A. Leitis, M. Liu, F. Yesilkoy, D. Choi, D. N. Neshev, Y. S. Kivshar, H. Altug, *Science* **2018**, 360, 1105.
- [180] A. Leitis, A. Tittl, M. Liu, B. H. Lee, M. B. Gu, Y. S. Kivshar, H. Altug, *Sci. Adv.* **2019**, 5, eaaw2871.
- [181] D. Yoo, N. Nguyen, L. Martin-moreno, D. A. Mohr, S. Carretero-palacios, J. Shaver, J. Peraire, T. W. Ebbesen, S. Oh, *Nano Lett.* **2016**, 16, 2040.
- [182] D. Rodrigo, O. Limaj, D. Janner, D. Etezadi, F. J. G. de Abajo, V. Pruneri, H. Altug, *Science* **2015**, 349, 165.
- [183] N. I. Landy, S. Sajuyigbe, J. J. Mock, D. R. Smith, W. J. Padilla, *Phys. Rev. Lett.* **2008**, 100, 207402.
- [184] S. Ogawa, D. Fujisawa, H. Hata, M. Uetsuki, K. Misaki, M. Kimata, *Appl. Phys. Lett.* **2015**, 106, 041105.
- [185] Y. Avitzour, Y. A. Urzhumov, G. Shvets, *Phys. Rev. B* **2009**, 79, 045131.
- [186] G. Dayal, X. Y. Chin, C. Soci, R. Singh, *Adv. Opt. Mater.* **2017**, 5, 1600559.
- [187] I. Hwang, M. Kim, J. Yu, J. Lee, J. Choi, S. A. Park, W. S. Chang, J. Lee, J. Jung, *Small Methods* **2021**, 5, 2100277.
- [188] O. Pe´rez-Gonza´lez, N. Zabala, A. G. Borisov, N. J. Halas, P. Nordlander, J. Aizpurua, *Nano Lett.* **2010**, 10, 3090.
- [189] T. Wang, Z. Dong, E. Huey, H. Koay, J. K. W. Yang, *ACS Photonics* **2019**, 6, 1272.
- [190] W. Sparreboom, A. Van Den Berg, J. C. T. Eijkel, *Nat. Nanotechnol.* **2009**, 4, 713.
- [191] D. Mijatovic, J. C. T. Eijkel, A. Van Den Berg, *Lab Chip* **2005**, 5, 492.
- [192] R. He, A. Yamauchi, T. Suga, *Jpn. J. Appl. Phys.* **2018**, 57, 02BD03.
- [193] J. Xu, C. Wang, T. Wang, Y. Wang, Q. Kang, Y. Liu, Y. Tian, *RSC Adv.* **2018**, 8, 11528.
- [194] T. H. H. Le, T. Tanaka, *ACS Nano* **2017**, 11, 9780.
- [195] J. Xu, Z. Ren, B. Dong, X. Liu, C. Wang, Y. Tian, C. Lee, *ACS Nano* **2020**, 14, 12159.
- [196] A. Leitis, M. L. Tseng, A. John-herpin, Y. S. Kivshar, H. Altug, *Adv. Mater.* **2021**, 33, 2102232.
- [197] A. R. Vollertsen, D. de Boer, S. Dekker, B. A. M. Wesselink, R. Haverkate, H. S. Rho, M. Blom, R. Passier, A. van den Berg, A. D. van der Meer, M. Odijk, *Microsyst. Nanoeng.* **2020**, 6, 107.
- [198] G. A. Akceoglu, Y. Saylan, F. Inci, *Adv. Mater. Technol.* **2021**, 6, 2100049.
- [199] A. R. Vollertsen, A. Simone, D. V. Schwach, A. Van Den Berg, R. Passier, A. D. van der Meer, M. Odijk, *Biomed. Microdevices* **2021**, 23, 30.
- [200] J. Fritzsche, D. Albinsson, M. Fritzsche, T. J. Antosiewicz, F. Westerlund, C. Langhammer, *Nano Lett.* **2016**, 16, 7857.
- [201] P. S. Ditttrich, A. Manz, *Nat. Rev. Drug Discovery* **2006**, 5, 210.
- [202] M. Napoli, J. C. T. Eijkel, S. Pennathur, *Lab Chip* **2010**, 10, 957.
- [203] R. Hansen, H. Bruus, T. H. Callisen, O. Hassager, *Langmuir* **2012**, 28, 7557.
- [204] B. Špačková, J. N. Scott Lynn, J. Slabý, H. Šípová, J. Homola, *ACS Photonics* **2018**, 5, 1019.
- [205] N. S. Lynn, J. Homola, *Anal. Chem.* **2016**, 88, 12145.
- [206] T. M. Squires, R. J. Messinger, S. R. Manalis, *Nat. Biotechnol.* **2008**, 26, 417.
- [207] P. E. Sheehan, L. J. Whitman, *Nano Lett.* **2005**, 5, 803.
- [208] M. J. Heller, A. H. Forster, T. Eugene, *Electrophoresis* **2000**, 21, 157.
- [209] D. L. Graham, H. Ferreira, J. Bernardo, P. P. Freitas, J. M. S. Cabral, *J. Appl. Phys.* **2003**, 91, 7786.
- [210] C. Escobedo, A. G. Brolo, R. Gordon, D. Sinton, *Anal. Chem.* **2010**, 82, 10015.
- [211] D. R. Kim, X. Zheng, *Nano Lett.* **2008**, 8, 3233.
- [212] M. A. Unger, H. Chou, T. Thorsen, A. Scherer, S. R. Quake, *Science* **2000**, 288, 113.
- [213] D. Rodrigo, A. Tittl, A. John-herpin, O. Limaj, H. Altug, *ACS Photonics* **2018**, 5, 4903.
- [214] R. Gordon, D. Sinton, K. L. Kavanagh, A. G. Brolo, *Acc. Chem. Res.* **2008**, 41, 1049.

- [215] C. Escobedo, A. G. Brolo, R. Gordon, D. Sinton, *Nano Lett.* **2012**, 12, 1592.
- [216] F. Eftekhari, C. Escobedo, J. Ferreira, X. Duan, E. M. Girotto, A. G. Brolo, R. Gordon, D. Sinton, *Anal. Chem.* **2009**, 81, 4308.
- [217] A. Barik, L. M. Otto, D. Yoo, J. Jose, T. W. Johnson, S. Oh, *Nano Lett.* **2014**, 14, 2006.
- [218] C. Dai, Z. Lin, K. Agarwal, C. Mikhael, A. Aich, K. Gupta, J.-H. Cho, *Nano Lett.* **2020**, 20, 6697.
- [219] T. H. H. Le, A. Morita, K. Mawatari, T. Kitamori, T. Tanaka, *ACS Photonics* **2018**, 5, 3179.
- [220] A. Vázquez-Guardado, S. Barkam, M. Peppler, A. Biswas, W. Dennis, S. Das, S. Seal, D. Chanda, *Nano Lett.* **2019**, 19, 449.
- [221] V. Abraham, F. Mehta, B. Jimenez, A. Biswas, K. Ray, A. Baksh, S. Lee, N. Saraf, S. Seal, D. Chanda, *Nano Lett.* **2021**, 21, 7505.
- [222] S. Alcon, A. Talarmin, M. Debruyne, A. Falconar, V. Deubel, M. Flamand, *J. Clin. Microbiol.* **2002**, 40, 376.
- [223] A. Vázquez-guardado, A. Safaei, S. Modak, D. Franklin, D. Chanda, *Phys. Rev. Lett.* **2014**, 113, 263902.
- [224] S. Halldórsson, E. Lucumi, R. Gómez-sjöberg, R. M. T. Fleming, *Biosens. Bioelectron.* **2015**, 63, 218.
- [225] P. C. Thomas, S. R. Raghavan, S. P. Forry, *Anal. Chem.* **2011**, 83, 8821.
- [226] F. Yesilkoy, R. A. Terborg, J. Pello, A. A. Belushkin, Y. Jahani, V. Pruneri, H. Altug, *Light: Sci. Appl.* **2018**, 17152.
- [227] A. A. Yanik, M. Huang, O. Kamohara, A. Artar, T. W. Geisbert, J. H. Connor, H. Altug, *Nano Lett.* **2010**, 10, 4962.
- [228] C. Z. J. Lim, Y. Zhang, Y. Chen, H. Zhao, M. C. Stephenson, N. R. Y. Ho, Y. Chen, J. Chung, A. Reilhac, T. P. Loh, C. L. H. Chen, H. Shao, *Nat. Commun.* **2019**, 10, 1144.
- [229] D. Conteduca, I. Barth, G. Pitruzzello, C. P. Reardon, E. R. Martins, T. F. Krauss, *Nat. Commun.* **2021**, 12, 3293.
- [230] M. Iwanaga, *Biosens. Bioelectron.* **2021**, 190, 113423.
- [231] M. Iwanaga, *Biosensors* **2021**, 11, 33.
- [232] J. J. S. Rickard, V. Di-pietro, D. J. Smith, D. J. Davies, A. Belli, P. G. Oppenheimer, *Nat. Biomed. Eng.* **2020**, 4, 610.
- [233] Z. Lao, Y. Zheng, Y. Dai, Y. Hu, J. Ni, S. Ji, Z. Cai, Z. J. Smith, J. Li, L. Zhang, D. Wu, J. Chu, *Adv. Funct. Mater.* **2020**, 30, 1909467.
- [234] C. Chen, Y. Li, S. Kerman, P. Neutens, K. Willems, S. Cornelissen, L. Lagae, T. Stakenborg, P. Van Dorpe, *Nat. Commun.* **2018**, 9, 1733.
- [235] J. Choi, J. Lee, J. Hee, *Biosens. Bioelectron.* **2020**, 169, 112611.
- [236] X. Miao, L. Yan, Y. Wu, P. Q. Liu, *Light: Sci. Appl.* **2021**, 10, 5.
- [237] D. Li, H. Zhou, X. Hui, X. He, X. Mu, *Anal. Chem.* **2021**, 93, 9437.



**Juan Wang** received a Ph.D. degree in 2020 at the University of Twente (The Netherlands). Currently, she is postdoctoral fellow in the group of Hybrid Nanosystems LMU Munich. The topics of her research include nanophotonics, photonic crystals, nanofabrication, and micro/nanofluidics for optofluidic sensing applications.



**Stefan Maier** heads the Chair in Hybrid Nanosystems LMU Munich and is also Lee-Lucas Chair in Experimental Physics at Imperial College London. He obtained his Ph.D. degree from Caltech in Applied Physics, and has since then worked at institutions in the UK and Germany.



**Andreas Tittl** holds a position as Emmy Noether Research Group Leader at LMU Munich, focusing on the design and experimental realization of novel metasurface concepts for enhanced light–matter coupling and ultrasensitive biodetection. After receiving his Ph.D. in Physics from the University of Stuttgart, he has worked as a postdoctoral researcher and Fellow at Ecole Polytechnique Fédérale de Lausanne (EPFL), where he pioneered the use of dielectric metasurfaces in biochemical spectroscopy.